Contents lists available at ScienceDirect

Journal of Hydrology

journal homepage: www.elsevier.com/locate/jhydrol

Research papers

An unbiased estimator of coefficient of variation of streamflow

Lei Ye [a], Xuezhi Gu [a], Dingbao Wang [b], Richard M. Vogel [c,*]

[a] School of Hydraulic Engineering, Dalian University of Technology, Dalian, China
[b] Department of Civil, Environmental, and Construction Engineering, University of Central Florida, Orlando, FL, USA
[c] Department of Civil and Environmental Engineering, Tufts University, Medford, MA, USA

ARTICLE INFO

This manuscript was handled by Andras Bardossy, Editor-in-Chief, with the assistance of Felix Frances, Associate Editor

Keywords:
Relative variability
Skewness
Intermittent
Periodic
Bimodal
Zero-inflated
Mixture

ABSTRACT

Given increasing demand for high frequency streamflow series (HFSS) at daily and subdaily time scales there is increasing need for reliable metrics of relative variability for such series. HFSS can exhibit enormous relative variability especially in comparison with low frequency streamflow series formed by aggregation of HFSS. The product moment estimator of the coefficient of variation C, defined as the ratio of sample standard deviation to sample mean, as well as ten other common estimators of C, are shown to provide severely downward biased and highly variable estimates of C for very long records of highly skewed and periodic HFSS particularly for rivers which exhibit zeros. Resorting to the theory of compound distributions, we introduce an estimator of C corresponding to a mixture of monthly zero-inflated lognormal distributions denoted as a delta lognormal monthly mixture ΔLN3MM model. Through monthly stratification, our ΔLN3MM model accounts for the seasonality, skewness, multimodality, and the possible intermittency of HFSS. In comparisons among estimators, our ΔLN3MM based C estimator is shown to yield much more reliable and approximately unbiased estimates of C not only for small samples but also for very large samples (tens of thousands of observations). We document values of C in the range of [0.18, 42,000] with a median of 1.9 and an interquartile range of [1.34, 3.75] for 6807 daily streamflow series across the U.S. from GAGES-II dataset, with the highest values of C occurring in arid and semiarid regions. A multivariate analysis and national contour map reveal that extremely large values of C, never previously documented, tend to occur in arid watersheds with low runoff ratios, which tend to also exhibit a considerable number of zero streamflows.

1. Introduction

Streamflow variability has a profound impact on nearly every aspect of water resource design, planning and management, and therefore its quantification plays a key role. Reliable and unbiased metrics for streamflow variability are needed in a range of activities including, but not limited to: classification of regional hydrologic homogeneity; goodness-of-fit assessments of hydrologic models; evaluation of impacts of climatic variability and change on hydrologic systems; and in a wide range of research activities which seek to understand the hydroclimatic mechanisms which give rise to hydrologic variability. Recent research has shown that high levels of hydrologic variability play a dominant role and create considerable obstacles relating to our ability to estimate very common hydrologic statistics such as the Pearson correlation coefficient (Barber et al., 2019) and the Nash-Sutcliffe efficiency goodness-of-fit metric (Lamontagne et al., 2020).

Among the existing measures of relative variability, the coefficient of variation, C, introduced by Pearson (1896, pp. 276–277), is now perhaps the most widely used metric. C is defined as $C = \sigma/\mu$ where μ and σ denote the population mean and standard deviation respectively, of the random variable of interest. The index C has been applied in many other research areas including business, engineering, science, medicine, economics, psychology and other social sciences as well as many other fields (Nairy and Rao, 2003; Kelley, 2007; Soliman et al., 2012). Alternatively, the standard deviation σ is often used for comparing the variability of samples, because it has the same units as the random variable of interest. However, when one's interest is in comparing the relative variability of several samples, each with different mean values, C is preferred to σ because it is nondimensional and thus accounts for differences in the mean of the samples. In finance, the inverse of C is commonly used as a measure of the performance of an investment portfolio (Knight and Satchell, 2005) and is often termed the risk to reward ratio.

We note at the outset, that C should only be computed for data

* Corresponding author.
E-mail address: richard.vogel@tufts.edu (R.M. Vogel).

https://doi.org/10.1016/j.jhydrol.2021.125954
Received 14 June 2020; Received in revised form 14 December 2020; Accepted 31 December 2020

measured on a ratio scale and would have no meaning for summarizing data on an interval scale (Velleman and Wilkinson, 1993). Ratio scale data are equally spaced data which exhibit a zero, whereas interval scale data are equally spaced data without a predefined zero point. Examples of ratio scale variables include streamflow, precipitation, and temperature measured in Kelvin. In contrast, most common temperature scales (e.g., Celsius, Fahrenheit etc.) are interval scales with arbitrary zeros, so C would be different depending on which scale is used. Most statistics including C, are meaningful for ratio data because their interpretation is unchanged when linear transformations are applied to the data. Other statistics such as means, standard deviations, and product moment correlations are meaningful for summarizing data on both ratio and interval scales.

1.1. Skewness and streamflow variability

Streamflow variability and skewness are linked. Vargo et al. (2010, Fig. 3) document the theoretical relationship between C and the coefficient of skewness γ for 36 probability distribution functions (pdfs). For two-parameter pdfs a unique relationship usually exists between C and γ (see Fig. 4 and discussion in Vogel and Fennessey, 1993). For example, for positively skewed Gamma and LN2 variables, γ is related to C via the relations $\gamma = 2C$, and $\gamma = 3C + C^3$, respectively. For more complex pdfs, with more than two parameters, there is usually no unique relationship between C and γ, however there still remains a linkage between the two, given by a two-dimensional region within the plot of C versus γ, as depicted in Fig. 3 of Vargo et al. (2010).

It is widely understood that streamflow observations exhibit both variability and skewness, yet due to numerous factors discussed in Section 1.5, the most common and widely used product moment estimators of the coefficients of variation C and skewness γ, exhibit both severe downward bias and variability, and are generally not to be trusted, even for sample sizes in the tens of thousands (see Vogel and Fennessey, 1993).

Obtaining reliable estimates of C for daily flow series constitutes the central challenge of this study. Initial efforts to obtain reliable estimates of C for daily streamflow series were made by Limbrunner et al. (2000) and Vogel et al. (2003) who applied an L-moment estimator of C based on a three-parameter lognormal distribution to flow series at 1571 watersheds across the U.S. Vogel et al. (2003) reported values of C for daily flow series ranging from approximately 0.5 to 10,000 with a median value of 10, and an interquartile range from 3 to 33. We were unable to find examples of such high values of C reported for any other variables, across multiple disciplines, which in part explains the need for new methods introduced here.

1.2. Influence of aggregation on streamflow variability

In the past, many water resources design, planning and management problems relied on low frequency streamflow series (LFSS) such as annual and monthly series resulting from the temporal aggregation (average) of daily, hourly, or subhourly high frequency streamflow series (HFSS). All such LFSS exhibit much less variability than the HFSS from which they were created. Regardless of the random variable of interest, aggregation leads to a reduction in variability. Given our focus on streamflow variability it is instructive to first consider the impact of aggregation of independent and identically distributed series. The aggregation (i.e. taking the average) of any independent and identically distributed (iid) random variable X over n intervals leads to a drop in its standard deviation σ to $\sigma/\sqrt{n}$, so that the coefficient of variation of the aggregated variable denoted as C_n is reduced to $C_n = C/\sqrt{n}$. Assume a daily time scale as a reference and denote the corresponding C as C_1. Since average annual streamflows are known to exhibit values of C_{365} in the range of [0.2, 1.5] across the conterminous U.S. (see Vogel et al., 1998), one would expect C for daily streamflows to be in the range [3.8, 28.5] resulting from the relationship $C_1 = \sqrt{365}C_{365} \approx 19C_{365} \rightarrow [3.8, 28.5]$. These initial results are only very crude approximations because daily streamflows are neither identically distributed nor independent, and both of these factors affect the estimation of C, a central focus of this study.

1.3. The influence of periodicity on estimates of streamflow variability

Most streamflow statistics attempt to provide a summary of the statistical behavior of streamflow, as distinguished from its physical or deterministic characteristics. Daily streamflow is subject to numerous deterministic characteristics including a periodic component which is dominated by seasonal climatic conditions which can lead to intermittent and ephemeral streamflows and the occurrence of observations equal to zero. HFSS, such as hourly streamflow, may be subject to other forms of periodic behavior such as diurnal variations.

In a recent study closely related to this study, the need to account for periodicity when estimating sample statistics of daily streamflow series was documented by Lamontagne et al. (2020) in their Monte-Carlo experiments which evaluated the sampling variability of estimates of the goodness-of-fit metric termed efficiency E. Fig. 4 of Lamontagne et al. (2020) documents that accounting for the periodic behavior of daily streamflow led to marked reductions in the variability of estimates of E when compared with estimators of E which did not account for streamflow periodicity.

1.4. The influence of zeros on streamflow variability

Zero streamflows are defined as streamflow below the measurement threshold, which is approximately 0.01 cfs in the U.S. (Granato et al., 2017). Of the 20,438 U.S. Geological Survey (USGS) river gages evaluated by Granato et al. (2017), 36% of those gages had at least one occurrence of zero streamflow and 2.6% of those gages had more than 297 days per year (or 81.3%) of zero streamflow. According to Levick et al. (2008), ephemeral and intermittent streams make up approximately 59% of all streams in the United States (excluding Alaska), and over 81% in the arid and semi-arid Southwest according to the USGS National Hydrography Dataset. Such streams usually reside in the headwaters or major tributaries of perennial streams in the Southwest.

Since the occurrence of zero daily streamflow is so common, we introduce a model which accommodates their occurrence; such a model that allows for frequent zero-valued observations is known as a zero-inflated model. We document later using both a zero-inflated model and streamflow observations, that the occurrence of zero streamflows leads to considerable increases in C, requiring estimators of C that accommodate their occurrence.

1.5. The sampling properties of estimates of the coefficient of variation, C

All statistics have both a theoretical and empirical interpretation. For example, the sample mean $\bar{x}$ computed from a single sample of length n, is a sample estimate of the true or population mean μ. The theoretical sampling properties of $\bar{x}$ are known for any iid variable and can be summarized by the mean and variance of $\bar{x}$. Since $E[\bar{x}] = \mu$, $\bar{x}$ is said to be an unbiased estimator of μ. Barber et al. (2019) and Lamontagne et al. (2020) provided examples of the sampling properties of estimates of the correlation coefficient and the Nash-Sutcliffe efficiency, respectively.

The difference between the population C and the mean of estimates of C is often referred to as 'sampling bias' because it results from estimating the true population value by a finite sample. Wallis et al. (1974) first exposed the importance of sampling bias in their seminal paper "Just a moment". Bias results from the combination of numerous phenomena acting together. The occurrence of zeros, skewness, persistence, and seasonality characterizing HFSS lead to considerable challenges

associated with estimation of C. Kirby (1974) also derived an upper bound on the product moment estimator of C which, until this study, was only considered to be important for small samples.

Values of population C exceeding unity correspond to samples with extremely high skewness, leading to enormous downward bias in all ratio estimators commonly used in hydrology. For example, for the case of population C = 10, Vogel and Fennessey (1993) reported downward bias associated with conventional product moment estimator of C of about 40% and 80% for samples of length 10,000 from synthetic iid samples from lognormal and generalized Pareto distributions, respectively. Note that Limbrunner et al. (2000), Vogel et al. (2003) and this study all document that a value of C = 10 for daily streamflows is not uncommon.

It is well known that autocorrelation inflates the sampling variance of most statistics. Vogel et al. (1998) and Lombardo et al. (2014) analyzed the effect of the autocorrelation on the sampling properties of various moments and moment ratios, expanding the results of Wallis et al. (1974). One can think of the impact of autocorrelation as decreasing the effective sample size, so that in the limit, the sample size approaches unity as the autocorrelation approaches unity (which is the case for HFSS). Moreover, all ratio estimators are known to exhibit bias, which is induced by the fact that the numerator and denominator are often correlated random variables each with different sampling properties of their own, resulting in bias in estimation of the overall ratio.

All product moment ratio estimators are known to exhibit bias due to outliers, because very large/small observations, which are far away from the sample mean, exert much more influence than the other observations, due to the exponentiation involved in higher-order moments. In such instances, which occur frequently in daily streamflow series, observations do not exert the same weight, and single or few observations can dictate the value of the sample estimates. Vogel and Fennessey (1993, Fig. 3) documented the enormous impact of the largest observation even for very large samples of daily streamflows in the tens of thousands; they also discussed remarkably large downward bias associated with product moment estimates of skewness and by analogy the same would be true for kurtosis and all other higher order moment ratios. For highly skewed bivariate lognormal samples, Lai et al. (1999) concluded that significant upward bias in estimates of the Pearson correlation coefficient exist, and only begins to disappear for sample sizes in the range of 3–4 million observations. Barber et al. (2019) extend the results of Lai et al. (1999) to highly skewed and periodic hydrologic series, showing clearly that the ordinary product moment estimator of the Pearson correlation coefficient should generally be avoided for use with daily and sub daily streamflow series. Thus, there is ample evidence in the literature that new methods are needed to better estimate C for highly skewed hydrologic data, even for very large samples.

The study of the sampling bias associated with commonly used product moment ratio estimators of HFSS has received very little attention, which is surprising when one considers the increasing attention being given to the application of HFSS in water resource management activities. It is now commonplace for hydrologists to model streamflow at sub daily scales (including hourly and even sub hourly scales) for use in flood forecasting as well as for real-time stormwater and water quality management activities and in hillslope hydrology applications. For example, the National Water Model (Office of Water Prediction, 2017) provides hourly streamflow forecasts for any location within the U.S. With increasing focus on challenges relating to big data, combined with increasing access to graphical processing units, supercomputer resources and the internet of things, one can expect to see continuing development of new HFSS modeling and data acquisition approaches which will result in profound challenges associated with estimation of various summary statistics corresponding to zero-inflated, periodic and highly skewed HFSS. Examples of research which address such challenges include this study, as well as the two recent studies by Barber et al. (2019) and Lamontagne et al. (2020).

1.6. Study goals

The primary goals of this paper are (1) to develop and compare approximately unbiased estimators of C for use with highly skewed, periodic, and possibly intermittent daily flow series and (2) to apply those estimators to large samples of daily streamflow data to enable a better understanding of the influence of skewness, zeros, periodicity and other physical factors, on the relative variability of streamflow. We begin with a literature review of estimators of C, followed by introduction of zero-inflated and monthly mixture models to deal with periodicity, skewness and non-perennial rivers. Three classes of estimators of C are introduced. The first class of estimators account for the high degree of variability and skewness associated with daily streamflows. The second class of estimators account for both skewness and zero-inflation, while the third class of estimators account for skewness, zero-inflation and the periodicity of daily streamflows. Then, we perform Monte Carlo experiments which compare the behavior of these estimators of C, and finally we apply those estimators to observed daily flow series across the U.S. A multivariate analysis and contour map of estimates of C enable us to summarize some of the hydroclimatic mechanisms which drive daily streamflow variability. Summary and recommendations conclude this study.

2. Estimation of C – Literature review

Our review reveals that nearly all approaches to estimation of C and its sampling properties assume that the random variable of interest is independent and identically distributed (iid). Daily streamflow is neither independent, nor identically distributed, yet since this is the assumption behind every estimator of C we could locate, we begin with a review of the estimators of C which stem from this assumption.

Most literature on the sampling properties of estimators of C assume independent normally distributed variates, with extensive results for the approximate (McKay, 1932) and the exact sampling distribution of estimators of C (Hendricks and Robey, 1936) as well as confidence interval estimation and hypothesis testing (Johnson and Welch, 1940). Of particular interest here are the properties of estimators of C for non-normal populations, yet there are very few publications on this subject. Koopmans et al. (1964) developed analytical confidence intervals for lognormal distributions. Pang et al. (2005) developed confidence interval estimates of C for Weibull, lognormal, and gamma distributions. Amiri and Zwanzig (2010) described the use of resampling approaches based on the Bootstrap for computing confidence intervals for C for non-normal and non iid samples. While there are numerous publications which have introduced methods for construction of confidence intervals for C for non-normal populations, there is very little attention given to the development of unbiased estimators of C for non-normal and periodic populations, the central goal of this study.

Banik and Kibria (2011) compared numerous estimators of C for skewed distributions. Soliman et al. (2012) considered estimation of C for a Burr-XII distribution and Pang et al. (2008) considered estimation of C for a bounded random variable following a Beta distribution. Soliman et al. (2011) introduced a simulation-based approach to estimation of C for a censored Gompertz distribution.

By far the most common estimator of C is obtained using product moments so that

$$\widehat{C}_{PM} = \frac{s_x}{\overline{x}} \tag{1}$$

where $s_x^2 = \sum_{i=1}^{n}(x_i - \overline{x})^2/(n-1)$ and $\overline{x} = \sum_{i=1}^{n} x_i/n$. Kirby (1974) documented that $\widehat{C}_{Kirby} = v_x/\overline{x}$, with $v_x^2 = \sum_{i=1}^{n}(x_i - \overline{x})^2/n$ is bounded above with an algebraic upper bound equal to $\sqrt{n-1}$. Wallis et al. (1974) and Vogel and Fennessey (1993) documented that $\widehat{C}_{PM}$ is remarkably downward biased, with that bias increasing as the skewness increases and/or sample size decreases. Vogel and Fennessey (1993)

considered much larger sample sizes than Wallis et al. (1974), and reported that for highly skewed samples from lognormal and generalized Pareto models, $\widehat{C}_{PM}$ exhibits enormous bias and variance which does not disappear even for sample sizes in the tens of thousands. It is for this reason that Vogel and Fennessey (1993) and others have recommended the use of the L-moment ratio known as L-Cv, instead of C, because estimates of L-Cv are nearly unbiased, regardless of the distribution from which the samples arise. We elect to estimate and focus attention on C instead of L-Cv because C is still far more widely reported, applied and understood than L-Cv. Furthermore, it is much easier to provide a physical interpretation of C than L-Cv, and one of our goals is to explain the physical drivers of streamflow variability.

Breunig (2011) derived expressions for the bias and variance of $\widehat{C}_{PM}^2$ for a sample arising from any distribution. Breunig (2011) reported the bias in $\widehat{C}_{PM}^2$ as

$$Bias\left(\widehat{C}_{PM}^2\right) = E\left[\widehat{C}_{PM}^2\right] - C^2 = \frac{C^{3/2}}{n}\left[3C^{1/2} - 2\gamma\right] \tag{2}$$

where γ is the skewness of the observations of X. It would be difficult to use (2) to obtain $Bias(\widehat{C}_{PM})$, instead the reader is referred to Vogel and Fennessey (1993, Fig. 5) who report $Bias(\widehat{C}_{PM})$computed from Monte-Carlo experiments based on lognormal and generalized Pareto distributions.

2.1. Lognormal estimators of C:

Of particular interest in hydrology is the lognormal distribution, which may be the most widely used distribution for characterizing a very wide range of skewed hydrologic variables. Hydrologic applications of the lognormal distribution include the frequency analysis of low flows, floods and water quality data, flow duration curves, rainfall intensity-duration, waste load allocations, and the physical, chemical and microbiological properties of soils and other geophysical media including but not limited to hydraulic conductivity, soil water retention, pore radius, and pore capillary pressure (Chow, 1954; Stedinger, 1980; Parkin et al., 1988; among others).

Naturally the lognormal assumption is only an approximation, though importantly, it is a much better approximation than normality which is the assumption associated with most previous research concerning estimation of C. Vogel et al. (1998) considered estimation of C for annual streamflow series that are well approximated by a two-parameter lognormal distribution (LN2). In this case an attractive estimator is the maximum likelihood estimator

$$\widehat{C}_{LN2} = \sqrt{exp\left(v_y^2\right) - 1} \tag{3}$$

where $v_y^2 = \sum_{i=1}^{n}\left(y_i - \overline{y}\right)^2/n$ and $\overline{y} = \sum_{i=1}^{n} y_i/n$, with $y = ln(x)$. Another attractive lognormal estimator of C is based on the uniform minimum variance unbiased estimators (UMVUE) of the mean $\widehat{\mu}_{Finney}$ and variance $\widehat{\sigma}_{Finney}^2$ introduced by Finney (1941) which can be expressed as:

$$\widehat{C}_{Finney} = \frac{\widehat{\sigma}_{Finney}}{\widehat{\mu}_{Finney}} = \frac{\sqrt{e^{2\overline{y}}\left[g\left(2s_y^2\right) - g\left(\frac{n-2}{n-1}s_y^2\right)\right]}}{e^{\overline{y}}\, g\left(\frac{s_y^2}{2}\right)} \tag{4}$$

where again $y = ln(x)$ with $\overline{y} = \sum_{i=1}^{n} y_i/n$ and $s_y^2 = \sum_{i=1}^{n}\left(y_i - \overline{y}\right)^2/(n-1)$ and

$g_{(n)}(t) = \sum_{k=0}^{\infty}\frac{v^k(v+2k)}{v(v+2)\cdots(v+2k)}\left(\frac{v}{v+1}\right)^k\frac{1}{k!}t^k$ with $v = n-1$.

Parkin et al. (1988) compared the sampling properties of the estimators $\widehat{C}_{PM}$, $\widehat{C}_{LN2}$ and $\widehat{C}_{Finney}$ under lognormal sampling for $n \leqslant 100$ and found that $\widehat{C}_{Finney}$ exhibits significantly lower mean square error than both $\widehat{C}_{PM}$ and $\widehat{C}_{LN2}$, particularly for small n and large values of C. For large values of n, well in excess of 100, we expect $\widehat{C}_{LN2}$ and $\widehat{C}_{Finney}$ to have similar performance.

An approximately unbiased estimator for the LN2 distribution can be derived from Eq. (2) which yields an expression for $Bias\left(\widehat{C}_{PM}^2\right)$ as a function of both skewness and sample size. For a lognormal distribution the skewness γ is a function of C so that $\gamma = 3C + C^3$, which can be combined with (2) to obtain the following approximately unbiased estimator

$$\widehat{C}_{Breunig} = \sqrt{\widehat{C}_{PM}^2 - Bias\left(\widehat{C}_{PM}^2\right)} = \sqrt{\widehat{C}_{PM}^2 - \frac{C^{3/2}}{n}\left[3C^{1/2} - 2\gamma\right]}$$

$$\cong \sqrt{\widehat{C}_{PM}^2 - \frac{\widehat{C}_{Breunig}^{3/2}}{n}\left[3\widehat{C}_{Breunig}^{1/2} - 2\left(3\widehat{C}_{Breunig} + \widehat{C}_{Breunig}^3\right)\right]} \tag{5}$$

Eq. (5) must be solved for $\widehat{C}_{Breunig}$ using an iterative numerical approach such as a Newton Raphson algorithm.

An estimate of C can also be obtained by fitting a three-parameter lognormal ($LN3$) distribution resulting in the estimator

$$\widehat{C}_{LN3} = \frac{\sqrt{exp\left(2\overline{y} + s_y^2\right)\left(exp\left(s_y^2\right) - 1\right)}}{\widehat{\tau} + exp\left(\overline{y} + \frac{s_y^2}{2}\right)} \tag{6}$$

where $y = ln(x - \widehat{\tau})$ $\overline{y} = \frac{1}{n}\sum_{j=1}^{n} y_j$ $s_y = \sqrt{\frac{1}{n}\sum_{j=1}^{n}\left(y_j - \overline{y}\right)^2}$

and $\widehat{\tau} = \frac{x_{(1)}x_{(n)} - (x_{0.5})^2}{x_{(1)} + x_{(n)} - 2x_{0.5}}$

The expression for the lower bound $\widehat{\tau}$ in (6) is the attractive estimator introduced by Stedinger (1980) where $x_{(1)}$ and $x_{(n)}$ are the smallest and largest nonzero observations respectively, and $x_{0.5}$ is an estimate of the median of X. The condition $x_{(1)} + x_{(n)} - 2x_{0.5} > 0$ must be satisfied to obtain a reliable estimate of τ in (6). If this condition is not satisfied, we assume an LN2 model so that $\widehat{\tau} = 0$ and therefore$\widehat{C}_{LN3} = \widehat{C}_{LN2}$. In addition, whenever $\widehat{\tau} < 0$ using (6), we elected to set $\widehat{\tau} = 0$ to ensure that no negative streamflows could be generated later on in our Monte-Carlo experiments.

2.2. Kappa and Wakeby estimators of C

Blum et al. (2017) evaluated the goodness-of-fit of various pdfs to distributions of nonzero daily streamflow across the U.S. and found that good approximations to $F(x)$ include the four-parameter Kappa (KAP) distribution, as well as the three-parameter lognormal (LN3); however, they did not evaluate mixture distributions as we do later on in this study. Blum et al. (2017) also provide a detailed review of studies which have sought to approximate the pdf of daily flow series for various regions of the world. More recently, Brunner and Gilleland (2020) fit a separate Kappa distribution to the daily streamflows on each day of the year. Appendix A provides estimators of C for nonzero streamflow series corresponding to the four-parameter Kappa (KAP) distribution and a five-parameter Wakeby (WAK) distribution.

Note that we do not constrain the lower bound on the fitted KAP and WAK distributions to be zero, because this approach enables improvements in the 'goodness-of-fit' of the fitted distributions to the nonzero observations. Nonzero daily streamflow observations are not usually bounded by zero anyway, as there is often a measurement threshold, (such as 0.01 cfs; see Rantz et al., 1982, page 571) which represents the minimum streamflow measurement reported by the USGS. We employ L-moment estimators of the parameters of these pdfs based on the work of Hosking (1990) and Hosking and Wallis (1997) using the software

developed specifically for these purposes (Hosking, 2017). Appendix A derives L-moment estimators of C corresponding to the KAP and WAK distributions termed $\widehat{C}_{KAP}$ and $\widehat{C}_{WAK}$, respectively.

2.3. Mixture distributions for streamflow

As discussed in the introduction, intermittent and ephemeral streamflows are common and result in a mixture of random variables describing (1) the occurrence of zero streamflow and (2) the magnitude of positive streamflow. The occurrence of zero streamflows complicates hydrologic frequency analyses because it creates a discontinuity in the pdf of streamflow, thus requiring a mixture model to adequately capture the pdf of both zero and nonzeros. Baldwin and Lall (1999), Prairie (2006) and others have documented that annual, seasonal and other periodic variations in daily streamflow can lead to complex bimodal pdfs. Unlike single pdfs, mixture models provide a flexible approach to capture the potential multimodal behavior of streamflow. For this reason, mixture models are now widely used in flood frequency analysis and have been found to yield improved estimates of flood quantiles when compared to methods based on single pdfs (Yan et al., 2017; and Szulczewski and Jakubowki, 2018).

In summary, daily streamflow series exhibit two mixture processes: (1) a mixture of periodic components as well as (2) a mixture of zero and non-zero flows. A discrete–continuous distribution is needed to account for both the occurrence of zero streamflows and the strong deterministic signals associated with seasonal periodicity within the daily flow series which can give rise to multimodal behavior in the pdf. In the following section we introduce a mixture modeling approach for handling both the occurrence of zeros and periodicity when computing hydrologic summary statistics from daily flow series.

2.4. A zero-inflated lognormal mixture (ΔLN3) model for handling zeros and skewness

In addition to periodicity, and the occurrence of zeros, daily and sub-daily streamflows are known to exhibit extremely high values of skewness, thus any mixture distribution will need to provide a flexible accounting of skewness. Barber et al. (2019), Blum et al. (2017) and Limbrunner et al. (2000, Fig. 6) used L-moment diagrams to illustrate that LN2 and LN3 distributions provide a good and very good, respectively, first approximation to the pdf of daily streamflow observations, for hundreds of stations across the conterminous U.S. Other more complex distributions such as the four-parameter Kappa or five-parameter Wakeby distribution were found to provide even better fits (Blum et al., 2017), particularly when the model parameters are allowed to vary from day to day (Brunner and Gilleland, 2020). Unlike this study, none of the above cited studies accounted for the discontinuity in the pdf of daily streamflows which can occur with intermittent and ephemeral rivers.

Zero-inflated pdfs have been introduced to handle the occurrence of zeros, by modeling the streamflow process as a mixture of two processes (1) zero flows and (2) magnitude of non-zero values. For example, Guo et al. (2016) applied a zero-inflated lognormal model which they termed a mixed lognormal model for modeling daily streamflows. Similarly, Kedeem et al. (1990) and Shimizu (1993) applied a zero-inflated lognormal model to rainfall processes. Zero-inflated lognormal models were first introduced by Aitchison (1955) and are more recently referred to by Crow and Shimizu (1988) as the delta lognormal model. All such models to date, referred to as delta lognormal models, ΔLN2, are three parameter models which combine the LN2 model with a third parameter defined as the probability of a zero observation. Here we introduce a natural extension to ΔLN2, termed the ΔLN3, which combines an LN3 model with a probability of zero defined as $(1-\delta)$. We employ a ΔLN3, model because HFSS are known to exhibit both zero streamflow as well as the remaining positive streamflows which are typically greater than some positive lower bound τ which represents either the minimum measurement threshold or the minimum value of reported streamflow discharge. For example, the U.S. Geological Survey only report nonzero streamflow discharge measurements above a minimum value of 0.01 cfs (Rantz et al., 1982, page 571). Thus in addition to the mean and variance of the nonzero streamflows, (i.e. the two parameters of a LN2 model), the ΔLN3 model has two additional parameters: (1) the lower bound τ of the positive streamflows and (2) the probability of zero streamflow $(1-\delta)$.

Following the existing literature (Aitchison, 1955; Crow and Shimizu, 1988; Shimizu, 1993; Kedeem et al., 1990; Guo et al., 2016), we define the cumulative distribution function (cdf) of the mixture process X in month i as $F_i(x) = P_i[X \leqslant x]$ which is made up of the cdf of the zero daily streamflows in month i (given by the Heaviside step function, $H_i(x) = 0$ when $x < 0$ and $H_i(x) = 1$ otherwise) and the continuous cdf of the nonzero daily streamflows in month i, $G_i(x)$. We extend this model into a monthly mixture model in the next section. The cdf of the mixture of zero and nonzero streamflows in month i, denoted $F_i(x)$, is given by

$$F_i(x) = (1-\delta_i)H_i(x) + \delta_i G_i(x) \tag{7a}$$

which can be rewritten as:

$$F_i(x) = \begin{bmatrix} 0 & x < 0 \\ 1-\delta_i & x = 0 \\ 1-\delta_i & 0 < x \leqslant \tau_i \\ (1-\delta_i) + \delta_i G_i(x) & \tau_i < x \end{bmatrix} \tag{7b}$$

where τ_i is the lower bound of streamflow in month i and $1-\delta_i$ is the probability of a zero streamflow in month i.

Combining (7) with the fact that $E[X^k] = \int_{-\infty}^{\infty} x^k dG(x) = \delta \int_0^{\infty} x^k f(x) dx$, we obtain an expression for the coefficient of variation of daily flows in month i denoted $C_i = \sigma_i/\mu_i$ as a function of the coefficient of variation of the nonzero flows in month i termed $C_{NZ,i}$ and the probability of zero flows $1-\delta_i$ as

$$C_i = \sqrt{\frac{C_{NZ,i}^2 + 1 - \delta_i}{\delta_i}} \tag{8}$$

Note that this result holds for all distributions $G_i(x)$ and is not unique to the Δ*LN*2 and Δ*LN*3 models below. As an example of the increase in variability resulting from the occurrence of zeros, C_i increases from 1.1 to 4.4 for fixed $C_{NZ,i} = 1$ and probabilities of zero flows $1-\delta_i$ equal to 0.1 and 0.9, respectively. Thus, arid and semi-arid regions are expected to experience extremely high values of C_i.

When $G_i(x)$ in (7) is an LN3 cdf, X follows a ΔLN3 model in which case one can easily extend results for the ΔLN2 model from Aitchison (1955) to obtain the mean and variance in month i as

$$\mu_i = \tau_i + \delta_i exp\left(\mu_{y,i} + \frac{\sigma_{y,i}^2}{2}\right) \tag{9a}$$

$$\sigma_i^2 = \delta_i exp\left(2\mu_{y,i} + \sigma_{y,i}^2\right)\left[exp\left(\sigma_{y,i}^2\right) - \delta_i\right] \tag{9b}$$

where $\mu_{y,i}$ and $\sigma_{y,i}^2$ are the mean and variance of $y = ln(x - \tau_i)$ in month i with τ_i equal to the lower bound of the *LN*3 model in month i. We approximate the pdf of HFSS in a given month i, using the above four-parameter Δ*LN*3 model with moments given by (9) as shown in the next section.

2.5. A delta LN3 monthly mixture (ΔLN3MM) model for handling periodicity, zeros and skewness

Selecting and fitting a single pdf to daily streamflow series, as was done in the previous section and in many previous studies, is ill-advised because such series are not identically distributed due to their seasonal behavior. One expects the parameters of any pdf fit to daily streamflow

series to exhibit seasonal and possibly other periodic behavior, thus we chose to model daily streamflow series using a monthly mixture model, where the daily streamflows in each month are modeled by the four-parameter ΔLN3 model given in the previous section. The resulting model is termed a ΔLN3 monthly mixture (ΔLN3MM) model for daily streamflow. A more parsimonious seasonal model could be employed, but such an approach would require the definition of seasons which differ by hydro climatologic regime, adding a degree of subjectivity which could cloud our ability to draw definitive conclusions concerning the impact of periodicity on estimation of C. Other approaches to modeling seasonality, such as by fitting smooth periodic functions, should be considered in future studies. Since daily flow samples considered here are in the tens of thousands, we elected not to concern ourselves with the often-critical issue of parsimony.

The ΔLN3MM model involves fitting a separate ΔLN3 model to the daily flows in each month so that each month i is characterized by the four parameters of the ΔLN3 model given by its mean $\mu_{y,i}$, variance $\sigma^2_{y,i}$, lower bound τ_i, and probability of zero $1-\delta_i$ corresponding to the daily streamflows x and their transformed values $y = ln(x-\tau_i)$. We employ this 48-parameter ΔLN3MM model to generate synthetic streamflow series which are shown in Section 5.2 to better mimic the complex marginal distribution of daily streamflows than a single ΔLN3 model. We also show later how to exploit this ΔLN3MM model for obtaining improved estimators of C. The ΔLN3MM model will produce daily streamflows that no longer follow a ΔLN3 model, and nonzero daily streamflows that no longer follow a LN3 distribution, as usual for compound distributions (Dubey, 1970; Porporato et al., 2006; and others). Importantly the ΔLN3MM is able to model the distribution of extremely complex, periodic, highly skewed, multimodal, ephemeral and intermittent streamflows.

Consider a monthly mixture distribution made up of fitting a separate ΔLN3 distribution $f(x;\mu_i,\sigma_i,\tau_i,\delta_i)$ to the daily streamflows in each of i = 1,…12, months where X denotes the daily streamflow observations within month i, τ_i denotes the lower bound, $(1-\delta_i)$ denotes the probability of zeros of the fitted Δ*LN*3 distribution in month i, and μ_i and σ_i denote the mean and standard deviation of the streamflows X in month i given in (9). The resulting ΔLN3MM pdf of all the daily streamflows is given by

$$f(x;\mu_1,...,\mu_{12},\sigma_1,...,\sigma_{12},\tau_1,...,\tau_{12},\delta_1,...,\delta_{12}) = \sum_{i=1}^{12} w_i f_i(x;\mu_i,\sigma_i,\tau_i,\delta_i) \tag{10}$$

where $f(\,)$ denotes the overall pd of X, and $f_i(\,)$ denotes the Δ*LN*3 pdf of the streamflows X in month i, and $\sum_{i=1}^{12} w_i = 1$. Combining (10) with the facts that $E[X^k] = \int_0^\infty x^k f(x)dx$ and $\sigma^2 = E\left[(X-\mu)^2\right] = E[X^2]-\mu^2$ leads to

$$E[X] = \mu = \sum_{i=1}^{12} w_i \mu_i \tag{11a}$$

and

$$E\left[(X-\mu)^2\right] = \sigma^2 = \sum_{i=1}^{12} w_i\left(\mu_i^2+\sigma_i^2-\mu^2\right) \tag{11b}$$

Eq. (11) can be used to obtain the overall coefficient of variation $C = \sigma/\mu$ of the resulting fitted ΔLN3MM distribution. Note that one can fit more complex distributions than either an ΔLN2 or ΔLN3 distribution to the daily streamflows in each month as long as one can obtain estimates of both the mean and varianceμ_i and σ_i^2 of X for each of the 12 fitted distributions in (9).

2.6. Estimation of parameters of the ΔLN3MM model

In this section we document how to estimate the parameters and overall cdf corresponding to the ΔLN3MM model in Section 2.5. The cdf of the daily streamflows corresponding to the monthly mixture model is obtained by integration of (10) which leads to:

$$F(x;\mu_1,...,\mu_{12},\sigma_1,...,\sigma_{12},\tau_1,...,\tau_{12},\delta_1,...,\delta_{12}) = \sum_{i=1}^{12} w_i F_i(x;\mu_i,\sigma_i,\tau_i,\delta_i) \tag{12}$$

where $F(\,)$ denotes the cdf of all the daily streamflows X, and $F_i(\,)$ denotes the ΔLN3 cdf of the streamflows **X** in month i. Here we assume the same number of days in each month which leads to the fixed weights $w_i \cong 1/12$, however future work may benefit from use of maximum likelihood or Bayesian estimators of the mixture weights as recommended by McLachlan et al. (2019).

Efficient estimation of the cdf of all the streamflows $F(\,)$ in (12) is as follows. First we note that in a given month i, nonzero streamflows X follow an LN3 model so that in each month $y = ln(x-\tau_i)$ follows a different normal model where an attractive estimator of the lower bound τ_i in each month i is given by the Stedinger (1980) estimator given in (6). From (7), an efficient estimate of the cdf of all the streamflows in month i, $F_i(x)$ is then given by

$$\widehat{F}_i(x) = \begin{cases} 0 & x < 0 \\ 1-\widehat{\delta}_i & 0 \leqslant x \leqslant \tau_i \\ \left(1-\widehat{\delta}_i\right)+\widehat{\delta}_i\widehat{G}_i(y) & x > \tau_i \end{cases} \tag{13}$$

with

$$\widehat{\delta}_i = 1-\frac{m_i}{n_i} \qquad \widehat{G}_i(y) = \Phi_i\left(\frac{y-\bar{y}_i}{s_{y,i}}\right)$$

$$\bar{y}_i = \frac{1}{n_i-m_i}\sum_{j=1}^{n_i-m_i} ln\left(x_j-\widehat{\tau}_i\right) \quad s_{y,i} = \sqrt{\frac{1}{n_i-m_i}\sum_{j=1}^{n_i-m_i}\left(ln\left(x_j-\widehat{\tau}_i\right)-\bar{y}_i\right)^2}$$

where m_i is the number zero streamflows in month i, n_i is the total number of streamflow observations in month i, $y = ln\left(x-\widehat{\tau}_i\right)$ with $\widehat{\tau}_i$ given in (6) and $\Phi(\,)$ denotes the cdf of a standard normal variable. We are concatenating daily flows across the entire n period of record, so that m and n denote the total number of zeros and the total number of streamflows in the entire n year record. For example, if there were no zero flows in any month i so that $m_i = 0$ in every month i, then there would be roughly n/12 flows in each month. An estimate of the cdf of all the daily streamflows $F(x)$ in (12) is obtained from

$$\widehat{F}(x) = \sum_{i=1}^{12} \frac{1}{12}\widehat{F}_i(x) \tag{14}$$

with $\widehat{F}_i(x)$ given in (13).

2.7. Goodness-of-Fit of the fitted Δ LN3, Δ KAP, Δ WAK and Δ LN3MM models

An important contribution of this study involves documenting the improved goodness-of-fit of the monthly mixture model over numerous common single pdf's often advocated for modeling daily flow duration curves. Here we assess the goodness-of-fit of the various fitted zero-inflated models (also termed delta models), as well as the monthly mixture model fitted to streamflow observations. Any pdf for nonzero observations can be converted to a zero-inflated model (or delta model) by substitution of the pdf of the nonzero values $G(x)$ into (7). When $G(x)$

is an *LN*3, *KAP*, *WAK*, cdf then $F(x)$ in (7) corresponds to the Δ*LN*3, Δ*KAP*, and Δ*WAK* models which are all compared in this section with the Δ*LN*3*MM* model. We employ the same procedure, regardless of whether or not the flow series exhibit zeros. We employ the widely used probability plot correlation coefficient *PPCC*, to evaluate the goodness-of-fit (Stedinger et al., 1993) of the fitted pdfs to the streamflow observations. There are two types of *PPCC*s, one based on a quantile–quantile (Q-Q) probability plot, and another based on a probability-probability (P-P) plot (Gan and Koehler, 1990). We employ P-P plots instead of Q-Q plots, because daily and hourly streamflow quantiles vary over 3–5 orders of magnitude, thus *PPCC* estimates from such Q-Q plots suffer from the same type of systematic bias that ratio estimators of C, skewness and kurtosis are known to exhibit, particularly for data series with very high values of C as is the focus here (see Vogel and Fennessey, 1993).

Gan and Koehler (1990) describe *PPCC* hypothesis tests based upon P-P plots, where the percentiles associated with each of the ranked observations computed from the fitted distribution are plotted against their unbiased (Weibull) plotting positions. The *PPCC* statistic based on a P-P plot is the Pearson correlation between these two axes, both of which have values between 0 and 1. Using *PPCC* statistics based on P-P plots treats each observation with effectively equal weight and as a result is influenced far less by outliers than a *PPCC* based on a Q-Q plot. *PPCC* hypothesis tests require an assumption that the flows are iid, however, since we only employ this statistic as a relative goodness-of-fit metric, our comparisons do not depend on the iid assumption.

Estimates of $r = PPCC$ corresponding to the fitted Δ*LN*3, Δ*KAP*, Δ*WAK*, and Δ*LN*3*MM* models are obtained from the Pearson correlation estimator defined by

$$r = \frac{\sum_{j=1}^{n}\left(\widehat{F}(x_{(j)}) - \overline{\widehat{F}}(x_{(j)})\right)\left(p_j - \overline{p}_j\right)}{\sqrt{\sum_{j=1}^{n}\left(\widehat{F}(x_{(j)}) - \overline{\widehat{F}}(x_{(j)})\right)^2 \sum_{j=1}^{n}\left(p_j - \overline{p}_j\right)^2}} \tag{15}$$

where $\widehat{F}(x_{(j)})$ is obtained by substitution of the j[th] ordered value of x, denoted $x_{(j)}$, into the expression for the cdf of the distribution given in (7b) and (13), and $\overline{\widehat{F}}(x_{(j)})$ denotes their mean values, across all n observations at a site. In (15) p_j denotes the Weibull plotting position estimate of the cumulative probabilities given by$p_j = j/(n+1)$. Here a Weibull plotting position is ideally suited, because it yields an unbiased estimate of the cumulative probability associated with the observations, regardless of their pdf (Stedinger et al., 1993). When there are m zero flows among the n flows, then an estimate of the cumulative probability of a zero flow is obtained from$p_m = m/(n+1)$

2.7.1. P-P probability plot for Δ*LN*3, Δ*KAP*, Δ*WAK* models

Estimates of the cdf of all streamflows denoted $\widehat{F}(x_{(j)})$, is needed to compute $r = PPCC$ in (15) and can be computed for each of the three fitted zero-inflated Δ*LN*3, Δ*KAP*, and Δ*WAK* models from

$$\widehat{F}(x_{(j)}) = \begin{bmatrix} 0 & x < 0 \\ 1-\widehat{\delta} & 0 \leqslant x \leqslant \widehat{\tau} \\ (1-\widehat{\delta}) + \widehat{\delta}\widehat{G}(x_{(j)}) & x > \widehat{\tau} \end{bmatrix} \tag{16}$$

with $\widehat{\delta} = 1 - (m/n)$ where m is the overall number of zero observations and n is the overall sample size.

PPCC for Δ*LN*3 Model: Substitution of the cdf of the nonzero observations $\widehat{G}(y_{(j)}) = \Phi\left(\left(y_{(j)} - \overline{y}\right)/s_y\right)$ with $\overline{y} = \sum_{j=1}^{n-m} ln(x_j - \widehat{\tau})/(n-m)$and $s_y = \sqrt{\sum_{j=1}^{n-m}(ln(x-\widehat{\tau}) - \overline{y})^2/(n-m)}$ into (16) yields an estimate of the cdf $\widehat{F}(x_{(j)})$ for the Δ*LN*3model needed to compute the *PPCC* in (15).

PPCC for Δ*KAP* Model: Substitution of L-moment estimates of the *KAP* parameters α, κ, h,and ξ into (A2) yields an estimate of the cdf of the nonzero observations $\widehat{G}(x_{(j)})$ which can be substituted into (16) to yield an estimate of the cdf $\widehat{F}(x_{(j)})$ for an Δ*KAP* model, needed to compute the *PPCC* in (15).

PPCC for Δ*WAK* Model: An analytical form of the pdf and cdf of a *WAK* distribution does not exist, however, it is possible to estimate $G(x)$ by solving (A5) numerically for G. Substitution of L-moment estimates of the *WAK* parameters α, β, γ, θ, and ξ into (A5) combined with a numerical solution yields an estimate of the cdf of the nonzero observations $\widehat{G}(x_{(j)})$, which can be substituted into (16) to yield an estimate of the cdf $\widehat{F}(x_{(j)})$ for an Δ*WAK* model, needed to compute the *PPCC* in (15).

2.7.2. P-P probability plot for Δ*LN*3*MM* Model:

A P-P probability plot is constructed by first ranking all the nonzero daily streamflow observations denoted $x_{(j)} j = 1, 2, \ldots, (n-m)$ where $n = \sum_{i=1}^{12} n_i$ is the total record length of the daily flow series and $m = \sum_{i=1}^{12} m_i$ is the total number of zero observations. Each ordered daily flow $x_{(j)}$ corresponds to a transformed flow $y_{(j)} = ln\left(x_{(j)} - \widehat{\tau}_i\right)$ for $i = 1, 2, \ldots, 12$ and$j = 1, 2, \ldots, n$ where $\widehat{\tau}_i$ is given in (6). Under the LN3 hypothesis, X follows an LN3 distribution and $Y_{(j)} = ln(X_{(j)} - \tau_i)$ follows a normal distribution so that a P-P probability plot is obtained by plotting a Weibull plotting position estimate of the cumulative probabilities $p_j = j/(n+1)$ versus an estimate of the cumulative probability of the fitted mixture distribution for the j[th] observation obtained from (14) where one replaces the observation x with the ordered observation $x_{(j)}$ with $\widehat{F}_i(x_{(j)})$ given in (13). Analogous to replacing x with $x_{(j)}$ in (14), one replaces the observation y with the ordered observation $y_{(j)}$ in (13). The PPCC is then obtained by computing the Pearson correlation coefficient between the n values of the plotting positions p_j and $\widehat{F}(x_{(j)})$ obtained from (14).

3. Summary of estimators of C

Three classes of estimators of C are introduced in this study: (1) sample estimators based on the assumption that daily streamflow arises from a single distribution which is equivalent to the assumption of identically distributed streamflows, throughout the year, (2) sample estimators based on a single zero-inflated which assume two populations, one for zero flows and one for nonzero flows, and (3) a mixture model which combines monthly zero-inflated LN3 model with a monthly mixture model. The first class of estimators attempt to account for the high degree of variability and skewness associated with daily streamflows. The second class of estimators account for both skewness and the occurrence of zeros, while the third class of models account for skewness, zeros and the periodicity of daily streamflows.

3.1. Estimators of C based on a single distribution

Section 2 and Appendix A summarizes a suite of estimators which assume that all streamflows arise from a single pdf. Those sample estimators were denoted: $\widehat{C}_{PM}, \widehat{C}_{LN2}, \widehat{C}_{Finney}, \widehat{C}_{Breunig}, \widehat{C}_{LN3}, \widehat{C}_{KAP}$, and $\widehat{C}_{WAK}$ given in Eqs. (1), (3), (4), (5), (6), (A4) and (A6), respectively.

3.2. Estimators of C based on a single Zero-Inflated distribution

Eq. (8) documents the analytical relationship between C_i corresponding to all streamflows in a given month and the value of $C_{NZ,i}$ corresponding to only the nonzero observations in that month. If one assumes that daily streamflows arise from the same zero-inflated distribution in every month then (8) reduces to:

$$\widehat{C} = \sqrt{\frac{\widehat{C}_{NZ}^2 + 1 - \widehat{\delta}}{\widehat{\delta}}} \tag{17}$$

Three single zero-inflated models were considered previously including the ΔLN3, Δ KAP and the ΔWAK models. In each case, a value for $\widehat{C}_{NZ}$ corresponding to the nonzero observations was derived and denoted $\widehat{C}_{LN3}, \widehat{C}_{KAP}$, and $\widehat{C}_{WAK}$, in equations (6), (A4) and (A6), respectively. Substitution of each of those corresponding values of $\widehat{C}_{NZ}$ into (17) leads to the estimators $\widehat{C}_{\Delta LN3}, \widehat{C}_{\Delta KAP}$, and $\widehat{C}_{\Delta WAK}$, corresponding to the three zero-inflated distributions.

3.3. Estimator of C based on monthly Zero-Inflated distributions and the monthly LN3 mixture model

The model which is expected to perform best in this study is the ΔLN3MM model because it accounts for skewness, periodicity and zero streamflows, all factors which influence the variability of streamflow. Estimation involving a zero-inflated monthly mixture model in arid regions could lead to small sample estimation issues, even when dealing with long records of daily streamflow. Recall, it is not uncommon for ephemeral headwater streams to experience values of $(1-\delta)$ in excess of 0.8 or 0.9, in which case the number of non-zero streamflows could be quite small. For example, a 10-year record (n = 3,650) of daily streamflow with $1-\delta = 0.9$ results in only 365 nonzero streamflows or only 30 nonzero flows per month if they are distributed evenly. Christman (2019) documents that the naïve estimators of the Δ*LN3MM*model in (13) exhibit significant bias for small iid samples (i.e., <100 observations), and that the UMUVE estimators introduced by Aitchison (1955) are preferred, thus we incorporate them below into our Δ*LN3MM* estimator of C.

The theoretical expression for C corresponding to a monthly mixture model in (11) can be rewritten in the form of an estimator for the Δ*LN3MM* model, by combining various results from (9), (11) and (13) with those of Aitchison (1955) to obtain

$$\widehat{C}_{\Delta LN3MM} = \frac{\widehat{\sigma}}{\widehat{\mu}} = \frac{\sqrt{\sum_{i=1}^{12}\left(\widehat{\mu}_i^2 + \widehat{\sigma}_i^2 - \widehat{\mu}^2\right)/12}}{\sum_{i=1}^{12}\widehat{\mu}_i/12} \tag{18a}$$

where

$$\widehat{\mu}_i = \widehat{\tau}_i + \widehat{\delta}_i exp\left(\overline{y}_i\right) g_{(n_i-m_i)}\left(\frac{s_{y,i}^2}{2}\right) \tag{18b}$$

$$\widehat{\sigma}_i^2 = \widehat{\delta}_i exp\left(2\overline{y}_i\right)\left[g_{(n_i-m_i)}\left(2s_{y,i}^2\right) - \left(1-\frac{m_i}{n_i-1}\right) g_{(n_i-m_i)}\left(\frac{n_i-m_i-2}{n_i-m_i-1}\right) s_{y,i}^2\right] \tag{18c}$$

$$\widehat{\delta}_i = 1-(m_i/n_i)$$

where $g_{(n_i-m_i)}()$ is given in (4), m_i is the number zero streamflows in month i, n_i is the total number of streamflow observations in month i, and formulas for the sample mean $\overline{y}_i$ and sample variance $s_{y,i}^2$ of the values of $y = ln\left(x-\widehat{\tau}_i\right)$ in a given month i, are given in (13) and $\widehat{\tau}_i$ is given in (6) but here is only applied to the $n_i - m_i$ nonzero streamflows. Note once again, (18) assumes the same number of days in each month so that $w_i = 1/12$ for all months.

4. Results

In the following section we first evaluate and compare the goodness-of-fit of the various pdfs introduced for modeling daily streamflow observations at thousands of watersheds across the conterminous U.S. We also perform Monte Carlo experiments which evaluate the sampling properties (bias and RMSE) of the various estimators of C introduced previously with the goal of determining which estimator is best suited to use with HFSS. We then apply the estimator of C which performs best in those experiments to summarize the behavior of C and to determine those factors which influence the relative variability of streamflow.

4.1. Database of streamflows

Estimates of C were obtained for a subset of the GAGES-II database (Falcone, 2011) based on two criteria: 1) There are continuous discharge data for more than 20 years; and 2) The percentage of missing data is <5%. Table 1 uses square brackets to summarize various statistical and hydroclimatic characteristics of discharge data and drainage area for the 6886 watersheds considered. Record lengths range from [20, 120] years, or [7300, 43,827] days corresponding to a median of 47.4 years or 17,289 days; and the drainage areas *A*, range from 0.77 to 49,802 km^2 with a median of 525 km^2. The climate aridity ratio *AR*, defined as the ratio of potential evapotranspiration *PET*, to precipitation *P*, was obtained for each watershed from the PRISM dataset (PRISM Climate Group, 2017). The values of *AR* in Table 1 illustrate a very broad range of hydro-climatologic regimes, because according to the climatic classification system introduced by Ponce et al. (2000, Table 1), the values of $AR = PET/P$ reported in Table 1 range from approximately [0.1, 5.71] which corresponds to hydro-climatological conditions ranging from arid to super humid conditions. Note that energy-limited ($AR < 1$) basins are more common than water-limited ($AR > 1$) basins since the median *AR* is 0.68. This characterization is consistent with the probability of zero discharge 1-δ, which is higher in the water-limited regions than that in the energy-limited regions.

Values of the runoff ratio *RR*, defined as the ratio of runoff to precipitation, summarized in Table 1 were obtained from the GAGES-II database, and the median runoff ratio is 0.34. It is worth noting that the runoff ratio in 32 of the 6886 watersheds is greater than 1. The potential reasons for this include: 1) The watersheds are not closed basins and may be subject to groundwater inflows and/or possible water diversions into the basin; and 2) The areal rainfall data are underestimated since the rainfall stations may not be representative of their entire watersheds.

4.2. Goodness-of-Fit evaluations using P-P plots

Section 3.4 summarized our approach for evaluating the goodness-of-fit of the ΔLN3, ΔKAP, ΔWAK and ΔLN3MM models using P-P plots and the PPCC statistic. We emphasize at the outset, that we expect that the less parsimonious ΔLN3MM to exhibit much higher PPCC values than the other more parsimonious models. In many hydrologic applications parsimony is a paramount concern, however here sample sizes are very large (compared to say, flood frequency analysis) thus parsimony is not as important a concern as in small sample applications and our goal is to employ a model with a nearly perfect goodness-of-fit for all basins considered, so that the model can be used to both mimic streamflow variability and to enable unbiased estimation of C.

Unfortunately, we were only able to fit a KAP distribution to 4607 of

Table 1
Summary of 6886 GAGES II Watersheds Considered in this Study Using Square Brackets and a Representative Subset of 190 Watersheds Using Parentheses.

Watershed Characteristic	Range	Interquartile Range	Median
Record length in days, n	[7300, 43827]	[11014, 26572]	[17289]
	(7300, 43827)	(11042, 21773)	(16958)
Record length in years	[20, 120]	[30.17, 72.80]	[47.4]
	(20, 120)	(30.25, 59.65)	(46.5)
Probability of zero 1-δ	[0, 0.9990]	[0, 0.00243]	[0]
	(0, 0.7741)	(0, 0.046)	(0.001)
Drainage area A, (km^2)	[0.77, 49802]	[145, 1916]	[525]
	(5.38, 42041)	(93, 1178)	(322)
Climate aridity ratio, AR	[0.10, 5.71]	[0.54, 0.86]	[0.68]
	(0.15, 2.06)	(0.54, 0.82)	(0.67)
Runoff ratio, RR	[0, 1.67]	[0.20, 0.44]	[0.34]
	(0, 1.09)	(0.24, 0.47)	(0.37)

the 6886 watersheds. Fig. 1 uses boxplots of the PPCC statistic to compare the goodness-of-fit among the LN3, KAP, ΔKAP, and ΔLN3MM models at 4528 of the 6886 sites where all four models could be fit. Fig. 1 documents the considerable improvement in goodness-of-fit resulting from the ΔLN3MM model when compared to the LN3, KAP, and ΔKAP models. The difficulty of fitting a KAP distribution to daily streamflow observations has been experienced before (see Blum et al., 2017, and studies cited therein), thus we drop both the KAP and the ΔKAP model from further goodness-of-fit comparisons. However, we encourage others to consider seasonal or monthly mixture models based on a KAP model analogous to the recent work by Brunner and Gilleland (2020) who fit a separate KAP model to daily streamflows on each day.

An advantage of the LN3 models over the KAP models is that we were able to fit them at nearly all 6886 watersheds, though the LN3 model reduced to an LN2 model at 3287 sites where the lower bound τ was set to zero for the reasons described in our discussion of Eq. (6). Fig. 2 compares boxplots of PPCC values corresponding to the three LN3 models: LN3, ΔLN3, and ΔLN3MM at 6807 of the 6886 watersheds where all three models could be fit. We were unable to fit the ΔLN3MM at 79 watersheds due to the occurrence of all zero flows in some months. Importantly, Fig. 2 documents the considerable improvement in the goodness-of-fit of the 48-parameter ΔLN3MM model over both the four-parameter ΔLN3 model and the three-parameter LN3 model, which reinforces and quantifies the importance of accounting for both the occurrence of zeros and the periodicity of streamflow series.

Fig. 3 uses a scatterplot to compare the PPCC value corresponding to the ΔLN3MM and ΔLN3MM models and again, documents the nearly global and rather significant improvement in the goodness-of-fit of the ΔLN3MM model over the single ΔLN3 zero-inflated model.

4.3. Monte-Carlo experiments

The goal of this section is to perform controlled Monte-Carlo experiments which enable us to conclude which estimator of C denoted $\widehat{C}$, performs best in terms of its percent bias $\%Bias\left(\widehat{C}\right) = 100\left[\left(C - E\left[\widehat{C}\right]\right)/C\right]$, and it's percent root mean square error $\%RMSE\left(\widehat{C}\right) = 100\left[\sqrt{E\left[\left(C-\widehat{C}\right)^2\right]}/C\right]$. These are standard metrics used in the statistics literature to evaluate the precision and accuracy of any estimator. Due to the well-known fact that mean square error of an estimator is made up of the sum of its bias squared and its variance, one can easily show that $\left[\%RMSE\left(\widehat{C}\right)\right]^2 = \left[\%Bias\left(\widehat{C}\right)\right]^2 + \%Var\left(\widehat{C}\right)$, thus

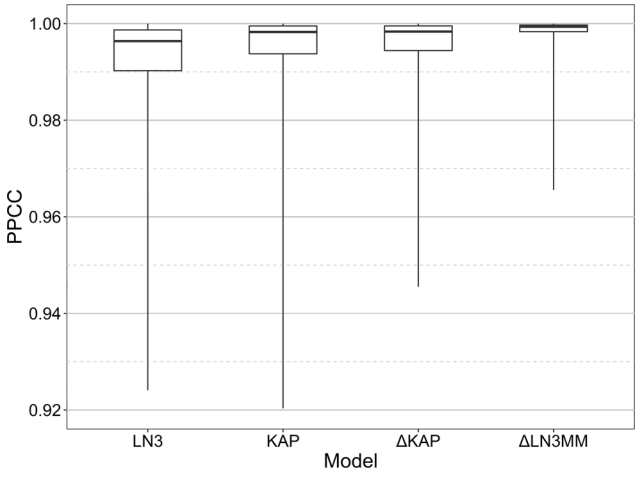

Fig. 1. Boxplots of the PPCC Goodness-of-Fit Statistic of LN3, KAP, ΔKAP and ΔLN3MM Models of Daily Streamflow at 4528 of the 6886 Watersheds Where All Four Models Could Be Fit.

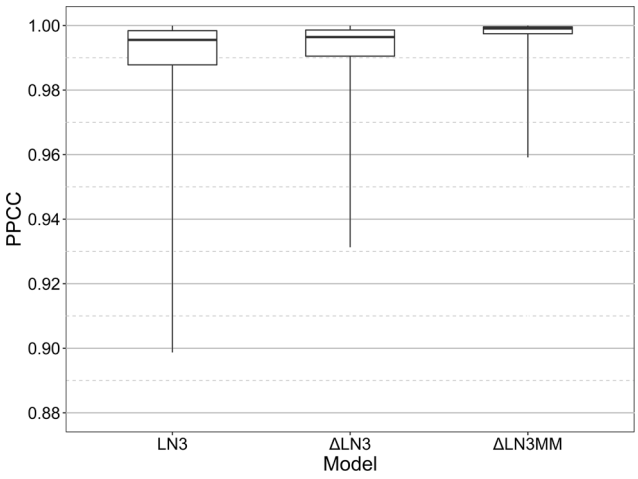

Fig. 2. Boxplots of the PPCC Goodness-of-Fit Statistic of LN3, ΔLN3 and ΔLN3MM Models of Daily Streamflow at 6807 of the 6886 Watersheds Where All Three Models Could Be Fit.

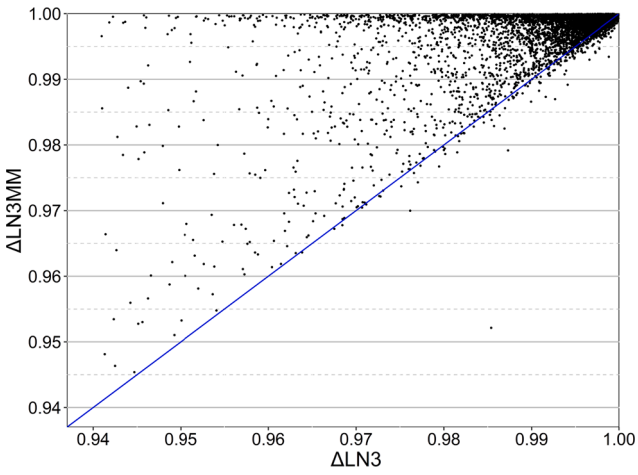

Fig. 3. The PPCC for the Fitted ΔLN3MM Model Versus the Fitted ΔLN3 Model at 6807 Stations.

it is only necessary to report any two of these indices to understand the general performance of the estimator $\widehat{C}$. To compute $\%Bias\left(\widehat{C}\right)$ and $\%RMSE\left(\widehat{C}\right)$ the true value C must be known or assumed. For the purposes of our Monte-Carlo experiments, we assume that values of $\widehat{C}_{\Delta LN3MM}$ in (18) computed from the complete records summarized in Table 1, are the true values of C at each site.

We selected a subset of 190 watersheds among the 6,886 watersheds for Monte-Carlo experiments due to the high computational burden associated with these experiments. The watershed characteristics of the chosen subset of 190 watersheds are summarized using parentheses in Table 1 for comparison with the 6886 watersheds shown using square brackets. The 190 watersheds were chosen so that (1) they all exhibited extremely high goodness-of-fit associated with the fitted ΔLN3MM model and (2) they reflect the distribution of $\widehat{C}_{\Delta LN3MM}$ which was observed among the 6886 sites. The ΔLN3MM PPCC values for the 190 sites ranged from 0.9966 to 0.9999 with a median value of 0.9996 and an interquartile range equal to [0.9993,0.9998] which is evidence of the extremely high goodness-of-fit associated with the ΔLN3MM model for these sites.

The distribution of the values of $\widehat{C}_{\Delta LN3MM}$ associated with the 190 selected stations ranged from 0.48 to 4072, with an interquartile range

from 1.2 to 8.2 and a median value of 2. Among the 190 sites, 14 stations had $\widehat{C}_{\Delta LN3MM} > 100$ and 4 stations had $\widehat{C}_{\Delta LN3MM} > 1000$. Among the 6807 sites for which we could fit the ΔLN3MM model, $\widehat{C}_{\Delta LN3MM}$ ranged from 0.19 to 42,000, with an interquartile range from 1.3 to 3.8 and a median value of 1.9. These results, combined with comparisons given in Table 1, indicate that the subset of 190 sites should reflect the overall behavior of the much larger set of 6807 watersheds. Note that the largest value of $\widehat{C}_{\Delta LN3MM}$ corresponding to the 6807 sites was much greater than the largest value among the 190 sites, because those extremely large values of $\widehat{C}_{\Delta LN3MM}$ correspond to sites with poor goodness of fit associated with the ΔLN3MM and hence were not included in the 190 sites. We generate synthetic streamflow series using the ΔLN3MM model with parameters estimated by applying (13) to the 190 streamflow records. The algorithm for generating 50 year (n = 18,250 days) synthetic streamflow records at each site, from the ΔLN3MM model is as follows:

1. For a given site, estimate the true values of the Δ*LN*3MM model parameters in each month *i*, from (13) so that $\delta_i = \widehat{\delta}_i, \mu_y = \overline{y}_i, \sigma_{y,i} = s_{y,i}$ with $\tau_i = \widehat{\tau}_i$ computed from (6),
2. Generate the uniform random variates $u_{i,j}$ over the interval [0, 1] where $i = 1, \ldots, 12$ months and $j = 1, \ldots, n_i$ where n_i is the total number of daily streamflows (both zero and nonzero) in month *i*, for the site under consideration.
3. Generate a total of n = 18,250 daily (50 year) streamflows $x_{i,j}$ at each site using

$$x_{i,j} = \begin{bmatrix} 0 & if \quad u_{i,j} \leqslant 1 - \delta_i \\ \tau_i + exp\left(\mu_{y,i} + z\left(u_{i,j}\right)\sigma_{y,i}\right) & otherwise \end{bmatrix} \tag{19}$$

where z() denotes a standard normal variate. Eq. (19) is used to generate $j = 1, \ldots, n_i$ daily streamflows in each month i. Figs. 4–7 illustrate boxplots of $\%Bias\left(\widehat{C}\right)$ and $\%RMSE\left(\widehat{C}\right)$ for the suite of estimators of C introduced here, when applied to the synthetic streamflow series generated at each of the 190 experimental sites. From this analysis, we note that $\widehat{C}_{\Delta LN3MM}$ is a considerable improvement over all other estimators considered in terms of both $\%Bias\left(\widehat{C}\right)$ and $\%RMSE\left(\widehat{C}\right)$.

Estimates of C values for some of the 190 stations could not be calculated from the ΔKAP or ΔWAK models, thus two sets of figures are included for %Bias and %RMSE: The %Bias (Fig. 4) and %RMSE (Fig. 6) could only be computed at 129 of the 190 stations using all 11 estimators; whereas, the %Bias (Fig. 5) and RMSE% (Fig. 7) could be computed for all 190 stations using the 7 methods which are not based on Kappa and Wakeby distributions. Importantly, both the %Bias and %RMSE of

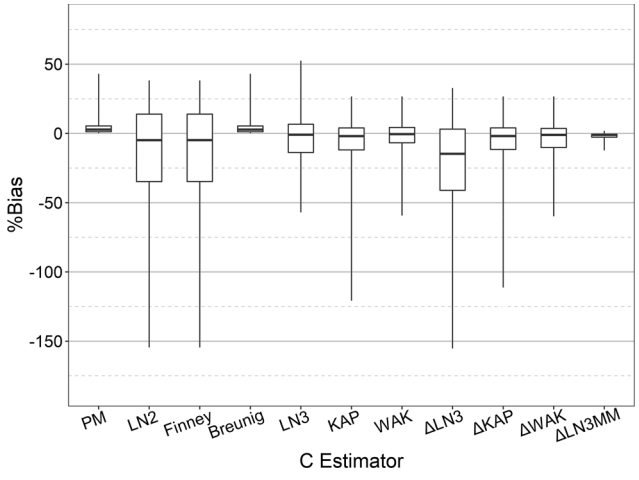

Fig. 4. %Bias of All 11 Estimators of C at 129 of the 190 experimental watersheds.

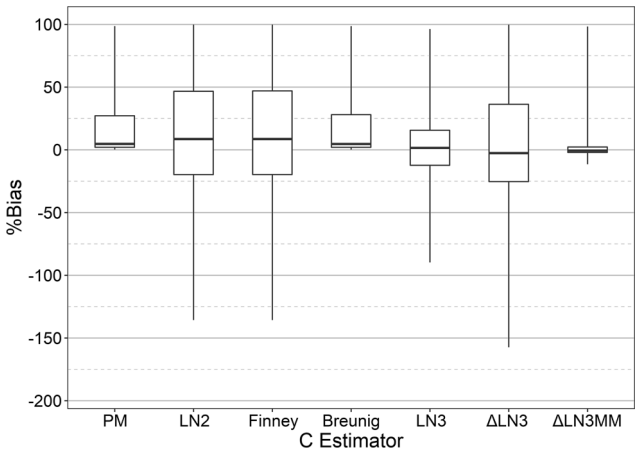

Fig. 5. %Bias for 7 Estimators of C at all 190 experimental watersheds.

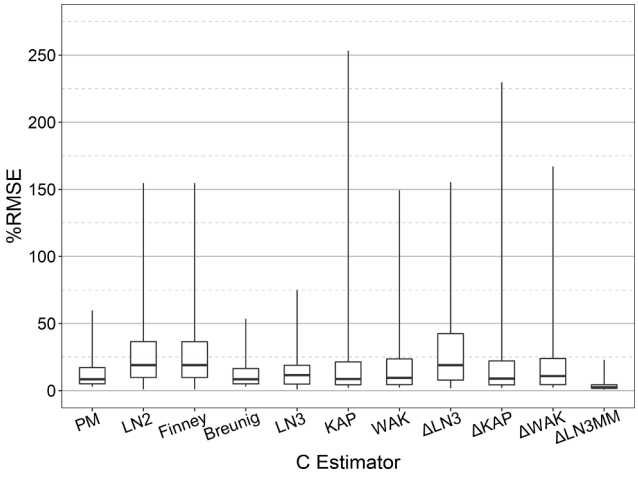

Fig. 6. %RMSE of All 11 Estimators of C at 129 of the 190 gage stations.

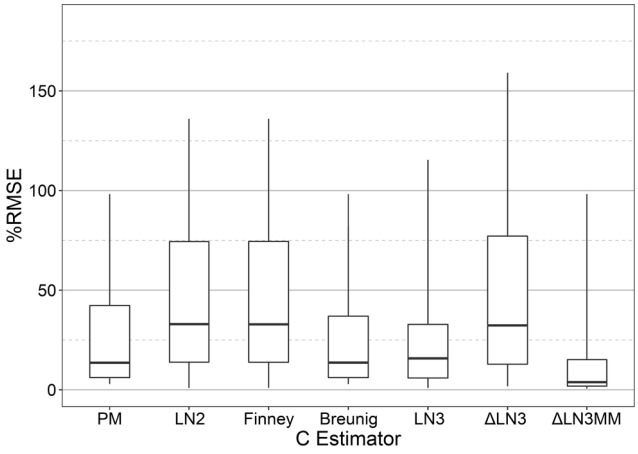

Fig. 7. %RMSE for 7 Estimators of C at all 190 experimental watersheds.

the ΔLN3MM estimator is smallest and generally much smaller than that of any other methods. The biases for the single distribution estimators $\widehat{C}_{Finney}$ and $\widehat{C}_{LN2}$ are the largest. The biases for the estimators $\widehat{C}_{PM}$ and $\widehat{C}_{Breunig}$ are always positive indicating that $\widehat{C}_{PM}$ and $\widehat{C}_{Breunig}$ are underestimated compared with the theoretical value.

Of considerable interest is the behavior of the most common esti-

mator of C, the product moment estimator $\widehat{C}_{PM}$. Fig. 8 illustrates a scatterplot of $\%Bias\left(\widehat{C}_{PM}\right)$ versus the assumed true value $C = \widehat{C}_{\Delta LN3MM}$ which illustrates as expected, that the enormous downward bias associated with $\widehat{C}_{PM}$ is greatest at sites with the highest values of $\widehat{C}_{\Delta LN3MM}$, which also tend to be those sites in arid and semi-arid regions as shown in Section 5. Fig. 9 is a plot of $\widehat{C}_{PM}$ versus $\widehat{C}_{\Delta LN3MM}$ for 6807 sites which illustrates that $\widehat{C}_{\Delta LN3MM}$ is able to cover a much broader range of values of C, than $\widehat{C}_{PM}$, giving us more sensitivity to the range of high values of C.

Fig. 9 highlights that there are many watersheds throughout the U.S. which have enormous values of $\widehat{C}_{\Delta LN3MM}$ in the hundreds and even thousands, whereas the naïve estimator $\widehat{C}_{PM}$ leads us to believe that there is an upper bound on C in the vicinity of 50. Recall Kirby's (1974) upper bound on $\widehat{C}_{PM}$ equal to $\sqrt{n-1}$ has an impact here, because the upper bounds on $\widehat{C}_{PM}$ corresponding to the range of sample sizes [7300, 43827] reported in Table 1, would range from [85, 209]. Kirby's bounds have an impact regardless of the stochastic structure of the observations and only require that the flows be nonnegative. Thus Kirby's upper bound on $\widehat{C}_{PM}$ could very well be causing some of the downward bias illustrated in Figs. 8 and 9. Together, Figs. 8 and 9 document that until the introduction of the estimator $\widehat{C}_{\Delta LN3MM}$ we have been unable to understand, depict and approximate an unbiased representation of the true relative variability of streamflow across broad hydroclimatic regimes.

5. Summary of behavior of estimates of C

Of considerable interest are the factors which give rise to such extremely large values of $\widehat{C}_{\Delta LN3MM}$ depicted in Fig. 9 across the conterminous U.S. Naturally there are many factors which would explain the gross variations in $\widehat{C}_{\Delta LN3MM}$ including, but not limited to: physical watershed characteristics, climatic characteristics, and numerous water management variables relating to withdrawals, diversions, return flows, reservoir operations, and other factors. It is beyond the scope of this initial study to consider all these factors; hence we only consider the impact of a few watershed and climatic characteristics. A natural sequel to this study would be a much more exhaustive study, with the goal of determining the key drivers of streamflow variability.

To this aim, we plotted $\widehat{C}_{\Delta LN3MM}$ versus the physical and statistical characteristics including: the probability of a zero $1-\delta$, watershed area A, runoff ratio *RR*, and aridity ratio *AR*. These scatter plots revealed no obvious discernable relationship except in the case of $\widehat{C}_{\Delta LN3MM}$ versus $1-\delta$, thus we only illustrate that scatterplot in Fig. 10 to save space and

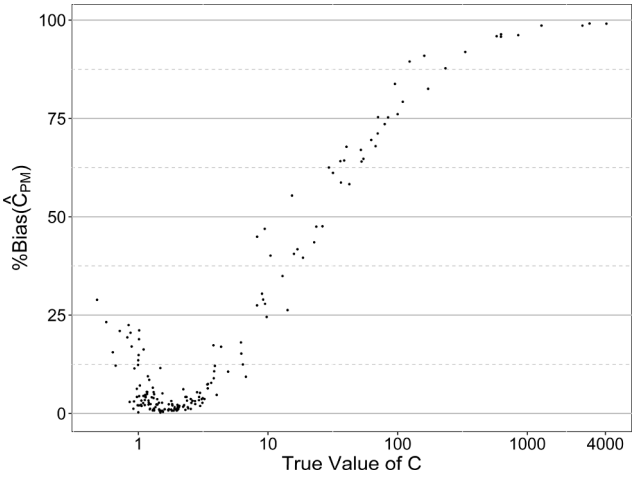

Fig. 8. The relation between $\%Bias\left(\widehat{C}_{PM}\right)$ and the true value of C.

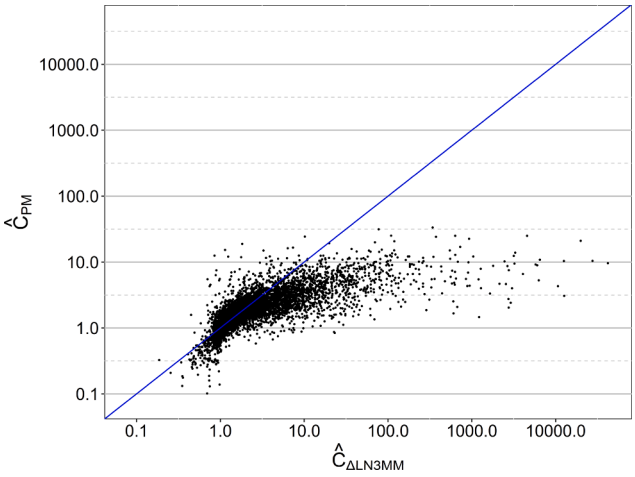

Fig. 9. The product moment estimator $\widehat{C}_{PM}$ Versus the Best Estimator $\widehat{C}_{\Delta LN3MM}$at 6807 Watersheds in the U.S.

we perform a more detailed multivariate analysis below.

The scatterplot in Fig. 10 indicates a strong relationship between $\widehat{C}_{\Delta LN3MM}$ and the probability of zeros $1-\delta$ for the 2166 watersheds that exhibited zeros. To further evaluate the multivariate relationship between $\widehat{C}_{\Delta LN3MM}$ and $1-\delta$, *A*, *RR* and *AR*, we fit the following multivariate model using ordinary least squares regression:

$$ln\left[\widehat{C}_{\Delta LN3MM}\right] = \beta_0 + \beta_1\Phi^{-1}[1-\delta] + \beta_2 ln[AR] + \beta_3 ln[RR] + \beta_4 ln[A] + \varepsilon \quad (20)$$

where $\Phi^{-1}[\,]$ is the inverse of a standard normal distribution, β_j, j = 0,..4 are model coefficients, and ε are model errors. The transformation $\Phi^{-1}[1-\delta]$ is only used to ensure that the probability of zero $1-\delta$, is bounded on the interval [0,1], whereas all other independent variables have no such constraints. Equation (20) was fit to 2166 of the 6807 of the watersheds summarized in Table 1 which exhibited zero streamflows. Table 2 summarizes estimates of the model coefficients and their corresponding t-ratios and p values associated with each explanatory variable. Diagnostic plots indicated relatively well behaved residuals which were roughly independent, homoscedastic and normally distributed. The high t-ratios and very low p-values in Table 2 along with the reasonably well behaved residuals enable us to conclude that all model coefficients are highly significant and stable. Influence statistics indicated that no watersheds exerted unusual influence on the model

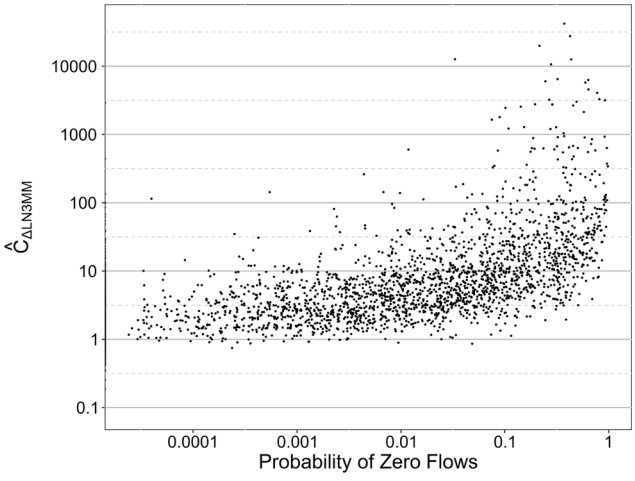

Fig. 10. $\widehat{C}_{\Delta LN3MM}$ versus the probability of zero flows at 2166 of the 6807 watersheds across the U.S. which exhibited zero daily streamflows.

Table 2
Model Coefficients of Fitted Regional Regression Model in Eq. (19).

Coefficient	Estimate	Explanatory Variable	t Ratio	p-Value
$\widehat{\beta}_0$	2.971	Intercept	29.56	0.000
$\widehat{\beta}_1$	0.7276	$\Phi^{-1}[1-\delta]$	30.28	0.000
$\widehat{\beta}_2$	0.3420	$ln[AR]$	4.25	0.000
$\widehat{\beta}_3$	−0.0748	$ln[RR]$	−2.67	0.008
$\widehat{\beta}_4$	0.0608	$ln[A]$	4.29	0.000

coefficient values. All variance inflation factors were below 2.0 revealing a general lack of multicollinearity among the explanatory variables. See Helsel et al. (2020) for background on influence statistics, variance inflation factors and other regression methods reported here.

The magnitude of the t-ratio is proportional to the explanatory power of its associated explanatory variable. The fitted model in (20) summarized in Table 2, resulted in an adjusted $R^2 = 42.2$. Substitution of the fitted model coefficients from Table 2 into (20) and exponentiation, yields a model for $\widehat{C}_{\Delta LN3MM}$:

$$\widehat{C}_{\Delta LN3MM} = exp\left[2.97 + 0.728\Phi^{-1}(1-\delta)\right] AR^{0.342} RR^{-0.0748} A^{0.0608} \quad (21)$$

We conclude that increases in $\widehat{C}_{\Delta LN3MM}$ result from increases in AR, A and the probability of zero flows $1-\delta$, and from decreases in RR. We also note that the exponents on AR, RR and A in Eq. (21) can be interpreted as nondimensional elasticities, so that a 1% increase in AR and A is expected to result in a 0.34% and a 0.06% increase in $\widehat{C}_{\Delta LN3MM}$, respectively. Similarly, a 1% increase in RR is expected to result in a 0.075% decrease in $\widehat{C}_{\Delta LN3MM}$.

Fig. 11 illustrates a contour maps of values of (a) $\widehat{C}_{\Delta LN3MM}$ and (b) $\widehat{C}_{PM}$ based on the 6.807 GAGES II watersheds summarized in Table 1. These maps were constructed using an inverse distance weighting interpolation method between the GAGES II gauging station locations. A comparison of the two maps in Fig. 11 reveals the remarkable differences in our understanding of the geographic variations in relative variability of daily streamflows revealed by these two different estimators of C particularly in arid and semi-arid regions. A comparison of Fig. 11a and b reveals that our estimator $\widehat{C}_{\Delta LN3MM}$ is able to represent an entirely new level of streamflow variability never before witnessed.

Analogous to the results of our multivariate analysis, the extremely high values of $\widehat{C}_{\Delta LN3MM}$ reported in Fig. 11, generally occur in arid and semi-arid regions of the southwestern U.S. and eastern Washington. Other instances of extremely high values of $\widehat{C}_{\Delta LN3MM}$ tend to correspond to locations with a high frequency of zero flows, as in southern Florida and some regions of the upper Midwest.

6. Impact of persistence on the behavior of estimates of C

Previous sections have accounted for the influence of periodicity, skewness, intermittent and ephemeral streamflow conditions on the properties of C. In this section we discuss briefly the influence of persistence on flow variability. Evidence of streamflow persistence can be described by its autocorrelation structure, which is known to have an impact on the sampling properties of estimators of C, the topic of this section. Vogel et al. (1998) documented the impact of serial correlation of the flow sequences on both the bias and variance of various estimators of C. They derived an approximately unbiased estimator of C in their Eq. (18) for flows which arise from an LN2 lag-one autoregressive process and documented using Monte Carlo experiments that their analytical expressions provide good approximations to both the bias and variance of their recommended estimator. An evaluation of their bias correction for autocorrelation indicates that it is only important for small samples (i.e. $n \langle 100$), even when autocorrelations approache unity as is the case for daily and hourly streamflows. Since daily and hourly flow sequences usually have sample sizes well in excess of 100, we neglect the impact of serial correlation on bias and refer the reader to Vogel et al. (1998) for further information.

7. Conclusions and recommendations

This study has sought to improve our understanding of the behavior of, and our ability to estimate the coefficient of variation C of high frequency streamflow series (HFSS), such as daily and subdaily series. We have also documented the critical need to account for the high levels of periodicity, skewness and zero streamflows associated with HFSS, when attempting to estimate summary statistics of such series.

Although other measures of relative variability exist, we focus on C because it is easy to interpret and understand and is probably the most widely used index of relative variability in hydrology. Given the enormous impact of streamflow variability on nearly every aspect of water resource design, planning and management, this study has sought to provide unbiased and reliable estimates of C for daily streamflows at watersheds exhibiting a wide range of hydroclimatic conditions. Recent research has shown that knowledge of the magnitude of C plays a dominant role and creates considerable obstacles relating to our ability to estimate very common hydrologic statistics such as the Pearson correlation coefficient (Barber et al. 2019) and the Nash-Sutcliffe efficiency goodness-of-fit metric (Lamontagne et al., 2020).

Three classes of estimators of C are introduced in this study. The first class of estimators are the traditional estimators $\widehat{C}_{PM}, \widehat{C}_{LN2}, \widehat{C}_{Finney}, \widehat{C}_{Breunig}, \widehat{C}_{LN3}, \widehat{C}_{KAP}$, and $\widehat{C}_{WAK}$ which can account for the high degree of variability and skewness associated with HFSS, but only perform well when streamflows are identically distributed which is rarely the case. The second class of estimators $\widehat{C}_{\Delta LN3}, \widehat{C}_{\Delta KAP}$, and $\widehat{C}_{\Delta WAK}$, are based on the three zero-inflated models: $\Delta LN3, \Delta KAP$, and the ΔWAK which account for both skewness and the occurrence of zeros. Finally, we introduce the new and promising estimator $\widehat{C}_{\Delta LN3MM}$ which accounts for skewness, zeros and the periodicity of daily streamflows, all factors shown to be integral to reliable and unbiased estimation of C. Our findings are based on Monte-Carlo experiments based on both (1) long series of daily streamflows at 6886 GAGES II watersheds, as well as (2) synthetic daily streamflows generated from a zero-inflated lognormal mixture model which we term the $\Delta LN3MM$ model, and the following conclusions are reached:

1. ***On the probability distribution of daily streamflows***: Goodness-of-fit evaluations at thousands of watersheds across the conterminous U.S. indicate that the $\Delta LN3MM$ monthly mixture model provides an improved goodness-of-fit to the pdf of daily streamflow series over a wide range of common single distribution functions recommended by others, including zero-inflated versions of those distributions. Fig. 2 documents the consistent and considerable improvement in the goodness-of-fit of the 48-parameter $\Delta LN3MM$model over both the four-parameter $\Delta LN3$ model and the three-parameter $LN3$ models, which reinforces and quantifies the importance of accounting for both the occurrence of zeros and periodicity, in addition to the high skewness associated with daily streamflow series.
2. ***On the need for mixture models to account for seasonality:*** Our Monte-Carlo experiments reveal that among the eleven different estimators of C considered, the estimator $\widehat{C}_{\Delta LN3MM}$ based on the $\Delta LN3MM$ model, exhibited remarkably lower %Bias and %RMSE than any other estimator. Importantly, those controlled experiments documented that accounting for the seasonal nonstationarity in the flow series with a monthly mixture model led to dramatic reductions in both the %Bias and %RMSE when compared to all other estimators considered. Our zero-inflated $\Delta LN3MM$ model accounts for the extremely complex, periodic, highly skewed, multimodal, and possibly ephemeral and intermittent characteristics of HFSS which is

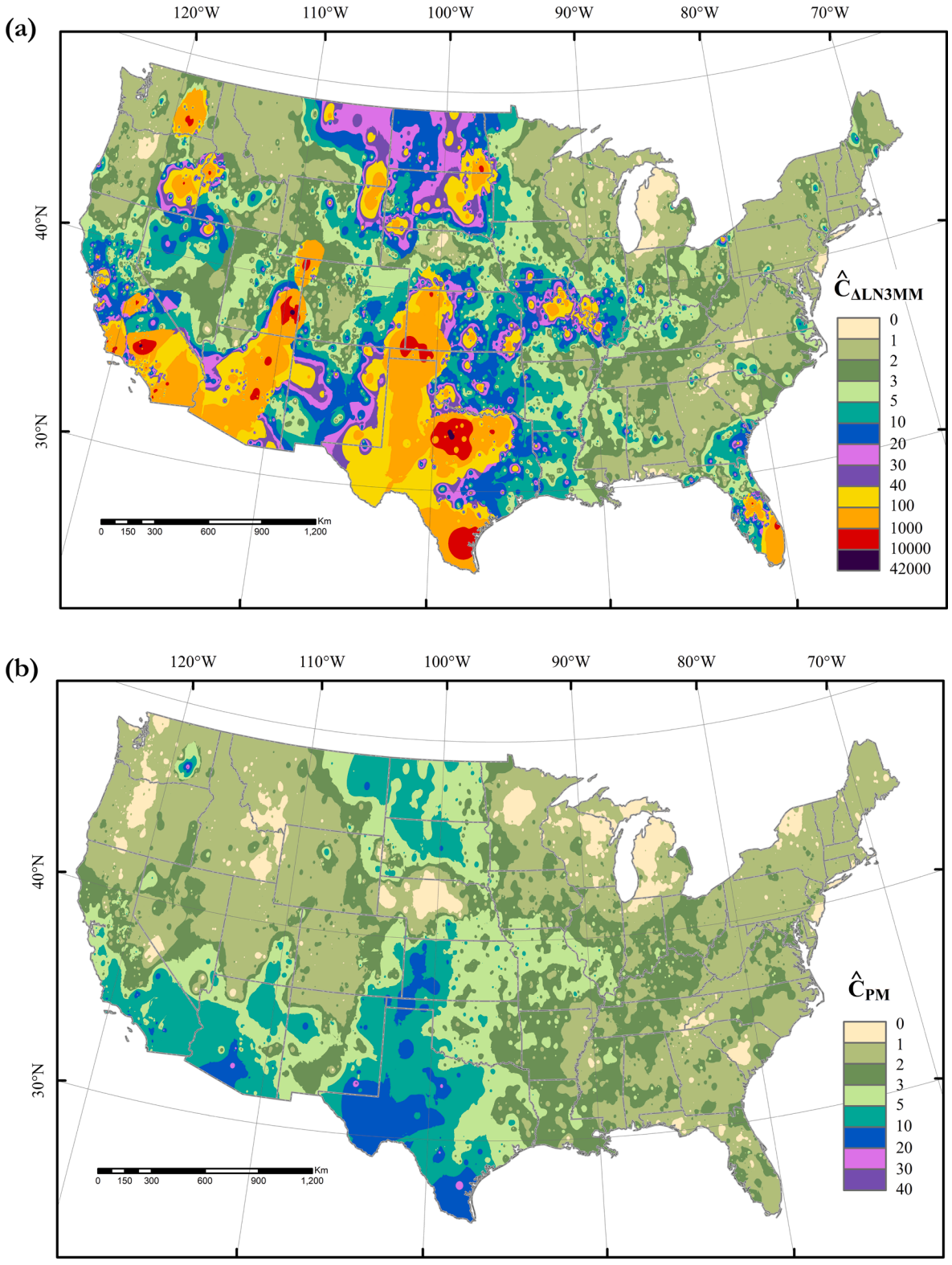

Fig. 11. Contour map of the estimators (a) $\hat{C}_{\Delta LN3MM}$ and (b) $\hat{C}_{PM}$based on daily streamflow series at 6807 GAGES II Watersheds.

shown to be necessary to obtain both unbiased and reliable estimates of C. Future studies should consider other methods for handling seasonality whether through different types of mixture models or through the introduction of periodic functions which approximate observed seasonality.

3. ***Extraordinary levels of streamflow variability are revealed from monthly mixture models:*** Extending the results documented by Vogel and Fennessey (1993) for C < 10, our experiments revealed downward bias in the traditional estimator of C termed $\hat{C}_{PM}$ which approached 100% for samples with extremely high values of C in excess of about 100. Comparison of values of the common product moment estimator $\hat{C}_{PM}$ with the estimator $\hat{C}_{\Delta LN3MM}$ at 6886 watersheds, in Fig. 11, led us to conclude that until now, we have been

unable to understand and depict the relative variability of streamflow C, across broad hydroclimatic regimes. Those comparisons reveal that $\widehat{C}_{\Delta LN3MM}$ is able to represent an entirely new and higher level of streamflow variability never before exposed or verified. Such high values of C in arid and semi-arid regions, imply that in such situations even estimates of the sample mean will exhibit such extraordinary variability that its use in such situations should be questioned. Therefore, improved zero-inflated monthly mixture estimators (or their equivalent) are needed for estimation of a host of other statistics (in addition to the mean and C) of daily and subdaily flow series in arid and semi-arid regions. Analogous to our findings concerning estimation of C, Lamontagne et al. (2020) document that an LN3 monthly mixture model is also quite useful for estimation of the Nash-Sutcliffe goodness-of-fit statistic when working with daily streamflows.

4. ***The impact of sample size, skewness, zeros and seasonality:*** Wallis et al. (1974) first identified the enormous bias and variability associated with $\widehat{C}_{PM}$ for iid skewed samples with small sample sizes (i.e. n $\langle$ 100) and Vogel and Fennessey (1993) found similar results for sample sizes in the tens of thousands from highly skewed iid samples with C < 10. This study is in some sense a sequel to those two studies, revealing that the extraordinary bias and variability associated with traditional estimators of C even for sample sizes in the tens of thousands, results from the high degree of skewness, periodicity and the occurrence of zeros associated with HFSS. What is unique to this study is our introduction of the $\Delta LN3MM$ model which accounts for the three factors: skewness, zeros, and periodicity, together, which enabled us to obtain unbiased and reliable estimates of C. Increases in skewness, periodicity and the likelihood of zeros were all shown to contribute to increases in both the %Bias and %RMSE of resulting estimators of C. We have also demonstrated that some of the downward bias in $\widehat{C}_{PM}$ is due, in part, to Kirby's (1974) upper bound, even with samples in the tens of thousands.
5. ***The Physical Causes of Streamflow Variability:*** A multivariate analysis of the 2166 streamgauges that experienced zero streamflow, revealed that increases in $\widehat{C}_{\Delta LN3MM}$ result from increases in the aridity ratio AR, drainage area A, and the probability of zero flows $1-\delta$, and from decreases in the runoff ratio RR. A comparison of national contour maps of $\widehat{C}_{\Delta LN3MM}$ and $\widehat{C}_{PM}$ documents the considerable improvement in our understanding of geographic variations in relative variability of daily streamflows resulting from the use of $\widehat{C}_{\Delta LN3MM}$, particularly in arid and semiarid regions. Those maps also illustrate the enormous geographic variations in the relative variability of daily flow series across the U.S.
6. ***Extensions and Recommendations:*** We expect future applications of zero-inflated mixture models to enable corresponding improvements in our ability to model the pdf and to estimate various summary statistics of daily flow series and other hydrologic series which exhibit high levels of skewness, periodicity and zeros. For example, given results of this study and the study by Brunner and Gilleland (2020), combined with recent recommendations by Blum et al. (2017), a natural extension to this study would be to evaluate the goodness-of-fit of zero inflated Kappa monthly mixture models for modeling the pdf of daily flow series. The vast and consistent improvement in goodness-of-fit of our$\Delta LN3MM$ model, over single pdf models could also be of considerable value to research on the application of flow duration curves (Castellarin et al. 2013). Analogous to this study, Lamontagne et al. (2020) introduced a bivariate monthly mixture modeling for daily streamflow observations and simulations, for the purpose of improving our ability to estimate model goodness-of-fit. We anticipate that zero-inflated monthly mixture models may be useful for estimating a wide range of common summary statistics including the mean, variance, skewness, kurtosis and correlation coefficients. We encourage future studies to consider alternative approaches to those considered here for accounting for skewness, periodicity and zeros when estimating hydrologic statistics such as C.

CRediT authorship contribution statement

Lei Ye: Software, Validation, Formal analysis, Investigation, Resources, Supervision, Visualization, Data curation, Project administration, Funding acquisition. **Xuezhi Gu:** Software, Formal analysis, Data curation, Investigation. **Dingbao Wang:** Conceptualization, Supervision, Investigation, Writing - review & editing. **Richard M. Vogel:** Conceptualization, Methodology, Formal analysis, Writing - original draft, Writing - review & editing, Validation, Visualization, Supervision.

Declaration of Competing Interest

The authors declare that they have no known competing financial interests or personal relationships that could have appeared to influence the work reported in this paper.

Acknowledgements

We are indebted to the late Nicholas C. Matalas, who provided some input on a very early version of this manuscript and who provided some of the inspiration for this work. We are also indebted to Francesco Serinaldi for his rigorous review of an early draft of this manuscript which led to considerable improvements in our presentation. We are also particularly indebted to Robert Hirsch for his extremely detailed and constructive comments. This work was partially supported by National Key Research and Development Program of China (no. 2016YFC0400906), the National Natural Science Foundation of China (no. 51709033) and the Fundamental Research Funds for the Central Universities (no. DUT20RC(3)019).

Appendix A. Estimators of C and $F(x)$ for Kappa and Wakeby distributions

The Kappa Distribution (KAP): Numerous investigators have suggested the four-parameter Kappa (KAP) distribution as the distribution of choice for fitting nonzero daily streamflow series (see Blum et al., 2017 for a recent review). The quantile function for a KAP distribution is

$$x(G) = \xi + \frac{\alpha}{k}\left[1 - \left(\frac{1-G^h}{h}\right)^k\right] \tag{A1}$$

where G denotes the cdf of the nonzero observations. The cdf of the nonzero observations needed in (16) to fit a ΔKAPdistribution is given by

$$G(x) = \left[1 - h\left(1 - \frac{k(x-\xi)}{\alpha}\right)^{1/k}\right]^{1/h} \tag{A2}$$

An estimate of the cdf $F(x)$ of all the streamflows (both zeros and nonzeros) corresponding to a ΔKAP is obtained by substitution of (A2) into (16)

using L-moment estimators of the four parameters of the nonzero *KAP* cdf.

Hosking (2017) provided algorithms for estimating the parameters of the *KAP* distribution using the method of L-moments. Hosking (1994) showed that all r[th] central moments of a *KAP* variable exists if $h \geqslant 0$ and $k \geqslant 0$. However, there are conditions for which only some of the r[th] moments exist such as for $r < -1/hk$ in which case they only exist for $h < 0$ and $k \geqslant 0$; and for $r < -1/k$ in which case they only exist if $k < 0$, thus we anticipate that situations may arise when C does not exist for the fitted *KAP* distribution.

Hosking (1994) provided analytical expressions which relate the parameters of a *KAP* distribution to its product moments. For most reasonable streamflow distributions, the *KAP* is limited to values of $h > 0$ in which case Hosking (1994) reported the r[th] moment of a *KAP* variate as

$$E[Y^r] = E\left[\left(1 - \frac{k(X-\xi)}{\alpha}\right)^r\right] = h^{-(1+rk)}\frac{\Gamma(1+rk)\Gamma\left(\frac{1}{h}\right)}{\Gamma\left(1+rk+\frac{1}{h}\right)} \tag{A3}$$

Using the fact that $X = \xi + \alpha(1-Y)/k$, the moments of X are easily derived from the moments of Y, so that one can compute the coefficient of variation of the nonzero values of X, using

$$C_{KAP} = \frac{\sigma_x}{\mu_x} = \frac{\alpha\sigma_y}{\xi k + \alpha(1-\mu_y)} = \frac{\alpha\sqrt{E[Y^2] - E[Y]^2}}{\xi k + \alpha(1-E[Y])} \tag{A4}$$

with $E[Y]$ and $E[Y^2]$ obtained from (A3). Substitution of L-moment estimators of the parameters α, κ, h, and ξ into (A4) leads to the estimator $\widehat{C}_{KAP}$.

The Wakeby Distribution (WAK) Houghton (1978) introduced the five-parameter Wakeby distribution as a distribution which could act as the parent distribution in hydrology, due to its extreme flexibility and ability to encompass and approximate the behavior of most other distributions in hydrology. Here we follow the parameterization of the five-parameter Wakeby (*WAK*) given by Hosking and Wallis (1997) with a quantile function given by

$$x(G) = \xi + \frac{\alpha}{\beta}[1-(1-G)^{\beta}] - \frac{\gamma}{\theta}[1-(1-G)^{-\delta}] \tag{A5}$$

where G denotes the cdf of the nonzero observations. Note that unlike the original version of a Wakeby distribution introduced by Houghton (1978), this version of a Wakeby distribution introduced by Hosking and Wallis (1997) always exhibits a lower bound at ξ so that $x \geqslant \xi$ always. An analytical form of the pdf and cdf of a *WAK* distribution does not exist, however, it is possible to estimate $G(x)$ by solving (A5) numerically for G.

Houghton (1978, eqn. (2) and (3)) derived the first four ordinary product moments of a Wakeby distribution as a function of its parameters, for the case when the quantile function takes the form: $x(F) = -a(1-F)^b + c(1-F)^{-d} + e$ which is different from the quantile function in (A5) given by Hosking and Wallis (1997). The two quantile functions are equivalent when $a = \alpha/\beta$, $b = \beta$, $c = \gamma/\theta$, $d = \theta$, and $e = \xi + (\alpha/\beta) - (\gamma/\theta)$ and that correspondence enables us to express C_{WAK} for the nonzero observations as

$$C_{WAK} = \frac{(\beta+1)(\theta-1)\sqrt{\frac{\alpha^2}{\beta^2(2\beta+1)} - \frac{\gamma^2}{\theta^2(2\theta-1)} - \frac{2\gamma\alpha}{\beta\theta(\beta-\theta+1)} - \frac{(\gamma\beta(1+\beta)+\alpha\theta(\theta-1))^2}{\beta^2\theta^2(1+\beta)^2(\theta-1)^2}}}{\gamma(1+\beta) + \alpha(1-\theta) + \xi(1-\theta)(1+\beta)} \tag{A6}$$

Note that there are numerous combinations of the model parameters for which either the mean and/or variance does not exist. For example, the mean does not exist if either $\beta = -1$ and/or $\theta = 1$. Similarly, the variance does not exist when β takes on values of 0, $-1/2$, or -1, or when θ takes on values of ½ or 1, etc. Thus it is entirely possible that fitted *WAK* distributions will have population values of C_{WAK} which simply do not exist. When one is unable to fit a five parameter *WAK* distribution, it may be possible to fit special cases of the distribution, such as the four parameter Wakeby distribution (see appendix to Hosking and Wallis (1997) for method). Substitution of the L-moment estimators of the five parameters a,β, γ, θ, and ξ into (A6) leads to the estimator $\widehat{C}_{WAK}$.

References

Aitchison, J., 1955. On the distribution of a positive random variable having a discrete probability mass at origin. J. Am. Stat. Assoc. 50, 901–908.

Amiri, S., Zwanzig, S., 2010. Assessing the coefficient of variations of chemical data using Bootstap method. J. Chemometrics 25, 295–300.

Baldwin, C.K., Lall, U., 1999. Seasonality of streamflow: The upper Mississippi River. Water Resour. Res. 35 (4), 1143–1154.

Banik, S., Kibria, B.M.G., 2011. Estimating the population coefficient of variation by confidence intervals. Commun. Stat. – Simul. Comput. 40 (8), 1236–1261. https://doi.org/10.1080/03610918.2011.568151.

Barber, C., Lamontagne, J.R., Vogel, R.M., 2019. Improved estimators of correlation and R^2 for skewed hydrologic data. Hydrol. Sci. J. https://doi.org/10.1080/02626667.2019.1686639.

Blum, A.G., Archfield, S.A., Vogel, R.M., 2017. The probability distribution of daily streamflow in the United States. Hydrol. Earth Syst. Sci. 21, 3093–3103. https://doi.org/10.5194/hess-21-3093-2017.

Breunig, R., 2011. An almost unbiased estimator of the coefficient of variation. Econ. Lett. 70, 15–19.

Brunner, M.I., Gilleland, E., 2020. Stochastic simulation of streamflow and spatial extremes: a continuous, wavelet-based approach. Hydrol. Earth Syst. Sci. 24, 3967–3982. https://doi.org/10.5194/hess-24-3967-2020.

*Castellarin, A., Botter, G., Hughes, D.A., Liu, S., Ouarda, T.B.M.J., Parajka, J., Post, D. A., Sivapalan, M., Spence, C., Viglione, A., Vogel, R.M., 2013. Prediction of flow duration curves in ungauged basins, Chapter 7 in Prediction in Ungauged Basins, Cambridge University Press, 496 pages.

Chow, V.T., 1954. The log-probability law and its engineering applications. Proc. ASCE, New York 80, 1–25.

Christman, M., 2019. Review of estimation methods for parameters of the delta-lognormal distribution. Technical Report. https://doi.org/10.13140/RG.2.2.13504.38408.

Crow, E.L., Shimizu, K. (Eds.), 1988. Lognormal Distributions: Theory and Applications. Marcel Dekker, Inc.

Dubey, S.D., 1970. Compound gamma, beta and F distributions. Metrika 16 (1), 27–31.

Falcone, J.A., (2011). GAGES–II—Geospatial attributes of gages for evaluating streamflow: U.S. Geological Survey metadata, also available at http://water.usgs.gov/GIS/metadata/usgswrd/XML/gagesII_Sept2011.xml.

Finney, D.J., 1941. On the distribution of a variate whose logarithm is normally distributed. Suppl. J. Roy. Stat. Soc. 7 (2), 155–161.

Gan, F.F., Koehler, K.J., 1990. Goodness-of-fit tests based on P-P probability plots. Technometrics 32 (3), 289–303.

Granato G.E., Ries, K.G., III, Steeves, P.A., 2017. Compilation of streamflow statistics calculated from daily mean streamflow data collected during water years 1901–2015 for selected U.S. Geological Survey streamgages: U.S. Geological Survey Open-File Report 2017–1108, 17 p., https://doi.org/10.3133/ofr20171108.

Guo, Y., Quader, A., Stedinger, J.R., 2016. Analytical estimation of geomorphic discharge indices for small intermittent streams. J. Hydrol. Eng. 21 (7), 04016015. https://doi.org/10.1061/(ASCE)HE.1943-5584.0001368.

Helsel, D.R., Hirsch, R.M., Ryberg, K.R., Archfield, S.A., Gilroy, E.J., (2020). Statistical methods in water resources: U.S. Geological Survey Techniques and Methods, book 4, chapter A3, 458 p., https://doi.org/10.3133/tm4a3.
Hendricks, W.A., Robey, W.K., 1936. The sampling distribution of the coefficient of variation. Ann. Math. Stat. 17, 129–132.
Hosking, J.R.M., 1990. L-moments: analysis and estimation of distributions using linear combinations of order statistics. J. Roy. Stat. Soc. B 52 (1), 105–124.
Hosking, J.R.M., 1994. The four parameter kappa distribution. IBM J. Res. Dev. 38 (3), 251–258.
Hosking, J.R.M., Wallis, J.R., 1997. Regional frequency analysis: an approach based on L-moments. Cambridge University Press, New York, USA, p. 224p.
Hosking J. R. M., (2017). L-Moments. R package, version 2.6. URL: https://CRAN.R-project.org/package=lmom.
Houghton, J.C., 1978. Birth of a parent: The Wakeby distribution for modeling flood flows. Water Resour. Res. 14 (6), 1105–1109.
Johnson, N.L., Welch, B.L., 1940. Application of the nonecentral t-distribution. Biometrika 31, 362–389.
Kedeem, B., Chiu, L.S., North, G.R., 1990. Estimation of mean rain rate: application to satellite observations. J. Geophys. Res. 95 (D2), 1965–1972.
Kelley, K., 2007. Sample size planning for the coefficient of variation from the accuracy in parameter estimation approach. Behav. Res. Methods 39 (4), 755–766.
Kirby, W., 1974. Algebraic boundedness of sample statistics. Water Resour. Res. 10 (2), 220–222.
Knight, J., Satchell, S., 2005. A re-examination of Sharpe's ratio for log-normal prices. Appl. Math. Finance 12 (1), 87–100.
Koopmans, L.H., Owen, D.B., Rosenblatt, J.I., 1964. Confidence intervals for the coefficient of variation for the normal and lognormal distributions. Biometrika 51 (1-2), 25–32.
Lai, C.D., Rayner, J.C.W., Hutchinson, T.P., 1999. Robustness of the sample correlation – The bivariate lognormal case. J. Appl. Math. Decis. Sci. 3 (1), 7–19.
Lamontagne, J.R., Barber, C.A., Vogel, R.M., 2020. Improved estimators of model performance efficiency for skewed hydrologic data. Water Resour. Res. 56 (9) https://doi.org/10.1029/2020WR027101.
Levick, L., Fonseca, J., Goodrich, D., Hernandez, M., Semmens, D.,Stromberg, J., Leidy, R., Scianni, M., Guertin, D.P., Tluczek, M., Kepner, W., 2008. The Ecological and Hydrological Significance of Ephemeral and Intermittent Streams in the Arid and Semi-arid American Southwest. U.S. Environmental Protection Agency and USDA/ARS Southwest Watershed Research Center, EPA/600/R-08/134, ARS/233046, p. 116.
Limbrunner, J.F., Vogel, R.M., Brown, L.C., 2000. Estimation of the harmonic mean of a lognormal variable. J. Hydrol. Eng. 5 (1), 59–66.
Lombardo, F., Volpi, E., Koutsoyiannis, D., Papalexiou, S.M., 2014. Just two moments! A cautionary note against use of high-order moments in multifractal models in hydrology. Hydrol. Earth Syst. Sci. 18, 243–255. https://doi.org/10.5194/hess-18-243-2014.
McKay, A.T., 1932. Distribution of the coefficient of variation and the extended "t" distribution. J. Roy. Stat. Soc. 95 (4), 695–698.
McLachlan, G.J., Lee, S.X., Rathnayake, S.I., 2019. Finite mixture models. Ann. Rev. Stat. Appl. 6, 355–378.
Nairy, K.S., Rao, K.A., 2003. Tests of coefficients of variation of normal population. Commun. Stat.—Simul. Comput. 32, 641–661.
Office of Water Prediction, 2017. The National Water Model. Office of Water Prediction, Tuscaloosa, AL.
Pang, W.-K., Leung, P.-K., Huang, W.-K., Liu, W., 2005. On interval estimation of the coefficient of variation for the three parameter Weibull, log-normal and gamma distribution: A simulation-based approach. Eur. J. Oper. Res 164 (2), 367–377.
Pang, W.K., Yu, B.W., Troutt, M.D., Hou, S.H., 2008. A simulation-based approach to the study of coefficient of variation of dividend yields. Eur. J. Oper. Res. 189, 559–569.
Parkin, T.B., Meisinger, J.J., Chester, S.T., Starr, J.L., Robinson, J.A., 1988. Evaluation of statistical estimation methods for lognormally distributed variables. Soil Sci. Soc. Am. J. 52, 323–329.
Pearson, K., 1896. Mathematical contributions to the theory of evolution? III. Regression, heredity and panmixia. Philos. Trans. Roy. Soc. A 187, 253–318.
Ponce, V.M., Pandey, R.P., Ercan, S., 2000. Characterization of drought across climate spectrum. J. Hydrol. Eng. ASCE 5 (2), 222–224.
Porporato, A., Vico, G., Fay, P.A., 2006. Superstatistics of hydroclimatic uctuations and interannual ecosystem productivity. Geophys. Res. Lett. 33 (15) https://doi.org/10.5194/hess-15-3207-2011.
Prairie, J.R., 2006. Stochastic nonparametric framework for basin wide streamflow and salinity modeling: Application for the Colorado River Basin. PhD. Dissertation. University of Colorado.
PRISM Climate Group, 2017. Parameter-elevation Relationships on Independent Slopes Model (PRISM). Northwest Alliance for Computational Science and Engineering at Oregon State University, Corvallis, Oregon, USA http://prism.oregonstate.edu.
Shimizu, K., 1993. A bivariate mixed lognormal distribution with an analysis of rainfall data. J. Appl. Meteorol. 32 (2), 161–171.
Soliman, A.A., Abd Ellah, A.H., Abou-Elheggag, N.A., Modhesh, A.A., 2012. Estimation of the coefficient of variation for non-normal model using progressive first-failure-censoring data. J. Appl. Stat. 39 (12), 2741–2758. https://doi.org/10.1080/02664763.2012.725466.
Soliman, A.A., Abd Ellah, A.H., Abou-Elheggag, N.A., Abd-Elmougod, G.A., 2011. A simulation-based approach to the study of coefficient of variation of Gompertz distribution under progressive first-failure censoring. Indian J. Pure Appl. Math. 42 (5), 335–356.
Stedinger, J.R., Vogel, R.M., Foufoula-Georgiou, E., 1993. Frequency Analysis of Extreme Events. Chapter 18, Handbook of Hydrology, McGraw-Hill Book Company, David R. Maidment, Editor-in-Chief.
Stedinger, J.R., 1980. Fitting lognormal distributions to hydrologic data. Water Resour. Res. 16 (3), 481–490.
Szulczewski, W., Jakubowski, W., 2018. The application of mixture distribution for the estimation of extreme floods in controlled catchment basins. Water Resour. Manage. 32 (10), 3519–3534.
Vargo, E., Pasupathy, R., Leemis, L.M., 2010. Moment-ratio diagrams for univariate distributions. J. Quality Technol. 42 (3), 276–286. https://doi.org/10.1080/00224065.2010.11917824.
Velleman, P.F., Wilkinson, L., 1993. Nominal, ordinal, interval, and ratio typologies are misleading. Am. Stat. 47 (1), 65–72. https://doi.org/10.1080/00031305.1993.10475938.
Vogel, R.M., Fennessey, N.M., 1993. L moment diagrams should replace product moment diagrams. Water Resour. Res. 29 (6), 1745–1752.
Vogel, R.M., Tsai, Y., Limbrunner, J.F., 1998. The regional persistence and variability of annual streamflow in the United States. Water Resour. Res. 34 (12), 3445–3459.
Vogel, R.M., Stedinger, J.R., Hooper, R.P., 2003. Discharge indices for water quality loads. Water Resour. Res. 39 (10), 1273. https://doi.org/10.1029/2002WR001872.
Rantz S.E., others, 1982. Measurement and computation of streamflow: Volume 2. Computation of Discharge, Geological Survey Water Supply Paper 2175, U.S. Geological Survey, Washington, D.C., p. 631.
Wallis, J.R., Matalas, N.C., Slack, J.R., 1974. Just a Moment! Water Resour. Res. 10 (2), 211–219.
Yan, L., Xiong, L., Liu, D., Hu, T., Xu, C.-Y., 2017. Frequency analysis of nonstationary annual maximum flood series using the time-varying two-component mixture distributions. Hydrol. Process. 31 (1), 69–89.